A displacement-based formulation for interaction problems between cracks and dislocation dipoles in couple-stress elasticity

K.P. Baxevanakis[1,*] and H.G. Georgiadis[2,3]

[1] *Wolfson School of Mechanical, Electrical and Manufacturing Engineering, Loughborough University, LE11 3TU, UK*

[2] *Mechanics Division, National Technical University of Athens, Zographou, GR-15773, Greece*

[3] *Office of Theoretical and Applied Mechanics, Academy of Athens, Greece*

Abstract: Interaction problems of a finite-length crack with plane and antiplane dislocation dipoles in the context of couple-stress elasticity are presented in this study. The analysis is based on the distributed dislocation technique where infinitesimal dislocation dipoles are used as strain nuclei. The stress fields of these area defects are provided for the first time in the framework of couple-stress elasticity theory. In addition, a new rotational defect is introduced to satisfy the boundary conditions of the opening mode problem. This formulation leads to displacement-based hyper-singular integral equations that govern the crack problems, which are solved numerically. It is further shown that this method has several advantages over the slope formulation. Based on the obtained results, it is deduced that in all cases the cracked body behaves in a more rigid way when couple-stresses are considered. The effect of couple-stresses is highlighted in a small zone ahead of the crack-tip and around the dislocation dipole, where the stress level is significantly higher than the classical elasticity prediction. Further, the dependence of the energy release rate and the configurational force exerted on the defect on the characteristic material length and the distance between the defect and the crack-tip is discussed. In the plane problems, couple-stress theory predicts either strengthening or weakening effects while in the antiplane mode a strengthening effect is predicted.

Keywords: Cracks; Dislocations; Dislocation Dipole; Disclinations; Microstructure; Couple-stress Elasticity; Hyper-Singular Integral Equations; Distributed Dislocation Technique; Peach-Koehler force.

[*] Corresponding author. Tel.: +44 (0) 1509 227030; fax: +44 (0) 1509 227648.
E-mail address: K.Baxevanakis@lboro.ac.uk (K.P. Baxevanakis)

1. Introduction

The macroscopic mechanical behavior of metals is significantly affected by phenomena that occur in the micro-scale. For instance, it is well accepted that crack growth is followed by damage formation around the main crack e.g. in the forms of microcracking and dislocation emission. Hence, interaction problems among cracks or between cracks and crystal defects have been studied with a variety of analytical and experimental techniques over the past decades (see indicatively Rice and Thomson (1974), Thomson (1987), Kobayashi and Ohr (1980), Majumdar and Burns (1981)). As discussed in Huang et al. (2006), the process of dislocation emission from crack-tips may manifest itself in emitted discrete dislocations (monopoles) or dislocation dipoles. In fact, dislocation dipoles are found in much higher densities than single dislocations during plastic deformation (Gilman, 1964). It is reminded that while discrete dislocations are *line defects*, dislocation dipoles are *area defects* of the crystal lattice.

Following our recent work on interaction problems between cracks and dislocations in the framework of couple-stress elasticity (Baxevanakis et al., 2017a, b), in this study we focus on interactions between finite-length cracks and dipoles of dislocations. The problems are studied in the context of couple-stress elasticity (or constrained Cosserat theory), which is the simplest theory of elasticity that accounts for effects induced by the material microstructure. It is noted that dislocation dipoles have not been studied using this generalized continuum theory before and so their elastic fields are derived for the first time herein. On the other hand, a few solutions are reported on the interaction problems under consideration in the context of classical isotropic elasticity. Specifically, Ballarini and Denda (1988) employed the complex potential method to derive the stress intensity factors at the tips of a finite-length crack due to the interaction with a plane dislocation dipole of random orientation. The analogous antiplane problem was studied by Lin et al. (1993). In addition, Wang and Lee (1992, 1993) identified the equilibrium states of a dislocation dipole near a semi-infinite crack and a criterion for emission of dipoles from its crack-tip.

In our previous investigations, the distributed dislocation technique (DDT) was employed and proved a very efficient method for the analysis of crack problems in couple-stress elasticity. It is mentioned that the term 'distributed dislocations' does not restrict the method

in using solely single dislocations to formulate a crack problem. In fact, any appropriate 'strain nucleus' that would produce a traction-free crack when distributed along its faces may be used. Based on these considerations, in this work we generalize the DDT in couple-stress theory and use dislocation dipoles as strain nuclei to describe the interaction problems. In analogy to electric dipoles, a dislocation dipole is defined as a pair of parallel dislocations that have equal and opposite sign Burgers vectors and are separated by a distance. Based on the separation distance, dislocation dipoles can be identified as *infinitesimal* or *finite* (Kroupa, 1965), as discussed in detail in Section 3. In crack problems, infinitesimal dislocation dipoles are used as strain nuclei.

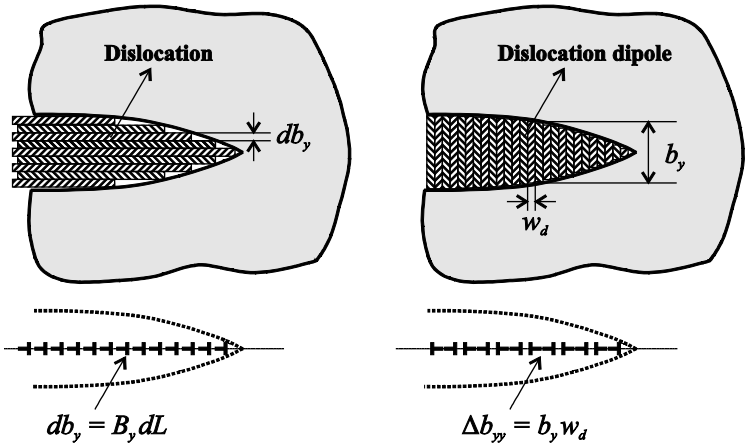

Fig. 1: Modeling of a mode I crack through a continuous distribution of discrete dislocations with Burgers vector db_y or through a distribution of infinitesimal dislocation dipoles of strength Δb_{yy} [reproduced after Dai (2002)].

The two approaches for the formulation of two-dimensional crack problems are schematically depicted in Fig. 1. As explained in Dai (2002), if the crack problem is formulated by a continuous distribution of discrete dislocations (db_y), the crack opening profile may be represented by a pile of narrow strips, each one corresponding to a climb dislocation. It is inferred that the crack opening displacement is the sum of Burgers vectors of all dislocations at any point along the crack faces. On the other hand, if the crack is modeled by a continuous distribution of infinitesimal dislocation dipoles (Δb_{yy}), the crack opening displacement is formed by an array of parallel thin strips, where each strip corresponds to an infinitesimal dislocation dipole. In this case, the normal crack face displacement at any point is equal to the Burgers vector of each dislocation dipole at the same location. In either case, the distributed defects should not be

misinterpreted as crystallographic defects but only as a way to create a traction-free crack. From a mathematical perspective, in the case of discrete dislocation distribution, the crack problem is formulated based on the gradient of the displacement field, which is used as the density of the governing integral equations (slope formulation). On the contrary, if dislocation dipoles are used to model the crack problem, the defect density corresponds to the crack face relative displacement (displacement formulation). Hence, in the latter case, the governing integral equations are in all cases hyper-singular which in turn means that the solution procedure is mathematically more involved since the evaluation of several integrals in the finite-part sense is required. However, the displacement-based formulation is advantageous for several reasons, as reported in the literature. Firstly, it is more direct and less computationally expensive than the slope formulation since no extra integration step is required to yield the displacement profile. This is particularly useful in problems where partial crack closure is observed (see e.g. Bjerkén and Melin, 2003). Also, the displacement function $u_i\left(x\right),\ i=1,\ 2,\ 3$ is continuous in the interval $-a \le x \le a$ while the slope is unbounded at the crack-tips. According to Chan et al. (2001), this formulation offers alternative and often simpler asymptotics of the integral equations kernels. Korsunsky and Hills (1995) compared the two methodologies and proved that fewer terms are required in the displacement-based method to achieve the same accuracy. It should be also added that this approach can be extended to axisymmetric and three-dimensional crack problems using dislocation loops as strain nuclei. Besides, either approach may be used to yield solutions in problems with complex geometries such as branched cracks and multiple crack configurations (TerMaath et al., 2006; Yavuz et al., 2006). Further details can be found in the studies of Korsunsky and Hills (1996), Dai (2002) and the treatise by Hills et al. (1996).

In the present work, we examine finite-length crack interactions with climb, glide, and screw dislocation dipoles. In all cases, the defects are placed along the crack plane so as not to induce crack closure effects. Furthermore, the defects are not emitted by the crack-tip. This configuration might be convenient for computations, but it does not fully represent the physical interaction problem. In Section 3, we derive the stress fields of the plane dislocation dipoles that need to be distributed along the crack faces in order to obtain the influence functions of the crack problems. Then, the three crack problems are presented in parallel in each section of the paper. As discussed in Baxevanakis et al. (2017a), in order to satisfy the boundary conditions of

the opening mode problems, both translational and rotational defects have to be distributed along the crack faces. Therefore, besides the distribution of infinitesimal climb dislocation dipoles we introduce a new rotational defect termed as *infinitesimal 'constrained' wedge disclination dipole*. Eventually, this problem is described by a system of coupled hyper-singular integral equations whereas the plane and antiplane shear problems are described by a single hyper-singular integral equation. In all cases, the equations are solved numerically. Finally, the evaluation of energetic quantities (J-integral and Peach-Koehler force) reveals an interesting 'alternating' behavior between strengthening and weakening effects when the material microstructure is considered, depending on the distance of the defect from the crack-tip and the ratio of the characteristic material length over the crack length.

2. Basic equations of couple-stress elasticity in plane and antiplane strain

In this section, we summarize the basic equations of the equilibrium theory of plane and antiplane strain within the linearized couple-stress theory of homogeneous and isotropic elastic solids. Couple-stress elasticity is the simplest theory of the so-called generalized continuum theories in which couple-stresses arise. For detailed presentations of the basic concepts of linear couple-stress elasticity we refer to the fundamental papers of Toupin (1962), Mindlin and Tiersten (1962) and Koiter (1964).

2.1 Plane strain

In this paragraph, we summarize the basic equations under static loading conditions in the plane strain case. For a body that occupies a domain in the $\left(x,\, y\right)$-plane under plane strain conditions, the two-dimensional displacement field is described as

$$u_x \equiv u_x(x,\, y)\ , \qquad u_y \equiv u_y(x,\, y)\ , \qquad u_z \equiv 0\ , \tag{1}$$

where the z axis is perpendicular to the $\left(x,\, y\right)$-plane.

For the kinematical description of the elastic body, the following expressions are defined for the strain tensor, the rotation vector, and the curvature tensor components

$$\varepsilon_{xx} = \frac{\partial u_x}{\partial x}\,, \qquad \varepsilon_{xy} = \varepsilon_{yx} = \frac{1}{2}\left(\frac{\partial u_x}{\partial y} + \frac{\partial u_y}{\partial x}\right), \qquad \varepsilon_{yy} = \frac{\partial u_y}{\partial y}\,, \tag{2}$$

$$\omega_z \equiv \omega = \frac{1}{2}\left(\frac{\partial u_y}{\partial x} - \frac{\partial u_x}{\partial y}\right), \tag{3}$$

$$\kappa_{xz} = \frac{\partial \omega}{\partial x}\,, \qquad \kappa_{yz} = \frac{\partial \omega}{\partial y}\,. \tag{4}$$

In Eq. (3) it is noticed that the normal component of the rotation is fully described by the distribution of the tangential displacements over the boundary. Therefore, the rotation vector ω_i in couple-stress elasticity is not independent of the displacement vector u_i.

Further, the expressions of force and moment equilibrium in the absence of body forces and body couples take the form

$$\frac{\partial \sigma_{xx}}{\partial x} + \frac{\partial \sigma_{yx}}{\partial y} = 0\,, \qquad \frac{\partial \sigma_{xy}}{\partial x} + \frac{\partial \sigma_{yy}}{\partial y} = 0\,, \qquad \sigma_{xy} - \sigma_{yx} + \frac{\partial m_{xz}}{\partial x} + \frac{\partial m_{yz}}{\partial y} = 0\,, \tag{5}$$

where σ_{pq} and m_{pq} are the components of the stress tensor and couple-stress tensor, which are both *asymmetric*.

Assuming a linear and isotropic material response the strain energy density takes the following form

$$W = \left(\lambda/2\right)\left(\varepsilon_{xx} + \varepsilon_{yy}\right)^2 + \mu\left(\varepsilon_{xx}^2 + 2\varepsilon_{xy}^2 + \varepsilon_{yy}^2\right) + 2\mu\ell^2\left(\kappa_{xz}^2 + \kappa_{yz}^2\right)\,, \tag{6}$$

where $\lambda = 2\mu\nu/\left(1-2\nu\right)$, μ is the shear modulus, ν is the Poisson's ratio and ℓ is the characteristic length introduced in couple-stress elasticity (Mindlin, 1963).

Then, the constitutive equations in the plane-strain case become

$$\varepsilon_{xx} = \big(2\mu\big)^{-1}\Big[\ \sigma_{xx} - \nu\big(\sigma_{xx} + \sigma_{yy}\big)\Big], \quad \varepsilon_{yy} = \big(2\mu\big)^{-1}\Big[\ \sigma_{yy} - \nu\big(\sigma_{xx} + \sigma_{yy}\big)\Big],$$
$$\varepsilon_{xy} = \big(4\mu\big)^{-1}\big(\sigma_{xy} + \sigma_{yx}\big) \tag{7}$$

and

$$\kappa_{xz} = \left(4\mu\ell^2\right)^{-1} m_{xz}\,, \qquad \kappa_{yz} = \left(4\mu\ell^2\right)^{-1} m_{yz}\,. \tag{8}$$

Accordingly, the non-vanishing components of the *asymmetric* stress tensor σ_{pq} in terms of the displacement components are given as

$$\begin{aligned}
\sigma_{xx} &= \big(\lambda + 2\mu\big)\frac{\partial u_x}{\partial x} + \lambda\frac{\partial u_y}{\partial y}, \qquad \sigma_{yy} = \big(\lambda + 2\mu\big)\frac{\partial u_y}{\partial y} + \lambda\frac{\partial u_x}{\partial x},\\
\sigma_{yx} &= \mu\left(\frac{\partial u_x}{\partial y} + \frac{\partial u_y}{\partial x}\right) + \mu\ell^2\left(\frac{\partial^3 u_y}{\partial x^3} - \frac{\partial^3 u_x}{\partial x^2\partial y} + \frac{\partial^3 u_y}{\partial x\partial y^2} - \frac{\partial^3 u_x}{\partial y^3}\right),\\
\sigma_{xy} &= \mu\left(\frac{\partial u_x}{\partial y} + \frac{\partial u_y}{\partial x}\right) - \mu\ell^2\left(\frac{\partial^3 u_y}{\partial x^3} - \frac{\partial^3 u_x}{\partial x^2\partial y} + \frac{\partial^3 u_y}{\partial x\partial y^2} - \frac{\partial^3 u_x}{\partial y^3}\right).
\end{aligned} \tag{9}$$

Combining now Eqs. (5) with (9), we obtain the following systems of *coupled* partial differential equations of the fourth order in terms of the components of the two-dimensional displacement field $\big(u_x,\, u_y\big)$

$$\frac{1}{1-2\nu}\frac{\partial}{\partial x}\left[2\big(1-\nu\big)\frac{\partial u_x}{\partial x} + \frac{\partial u_y}{\partial y}\right] + \frac{\partial^2 u_x}{\partial y^2} + \ell^2\left(\frac{\partial^4 u_y}{\partial x^3\partial y} - \frac{\partial^4 u_x}{\partial x^2\partial y^2} + \frac{\partial^4 u_y}{\partial x\partial y^3} - \frac{\partial^4 u_x}{\partial y^4}\right) = 0\,, \tag{10}$$

$$\frac{1}{1-2\nu}\frac{\partial}{\partial y}\left[2\big(1-\nu\big)\frac{\partial u_y}{\partial y} + \frac{\partial u_x}{\partial x}\right] + \frac{\partial^2 u_y}{\partial x^2} + \ell^2\left(\frac{\partial^4 u_x}{\partial x^3\partial y} - \frac{\partial^4 u_y}{\partial x^2\partial y^2} + \frac{\partial^4 u_x}{\partial x\partial y^3} - \frac{\partial^4 u_y}{\partial x^4}\right) = 0\,. \tag{11}$$

2.2 Antiplane strain

Consider now a body that occupies a domain in the $\big(x,\, y\big)$-plane under antiplane strain conditions. In this case, the displacement field reduces to

$$u_x = u_y = 0\ , \qquad u_z \equiv w \neq 0\ , \qquad w \equiv w(x,\, y). \tag{12}$$

The non-vanishing components of the strain tensor, the rotation vector, and the curvature tensor are defined as (Lubarda, 2003)

$$\varepsilon_{xz} = \frac{1}{2}\frac{\partial w}{\partial x}\ , \qquad \varepsilon_{yz} = \frac{1}{2}\frac{\partial w}{\partial y}, \qquad \omega_x = \frac{1}{2}\frac{\partial w}{\partial y}\ , \qquad \omega_y = -\frac{1}{2}\frac{\partial w}{\partial x}\ , \tag{13}$$

$$\kappa_{xx} = -\kappa_{yy} = \frac{1}{2}\frac{\partial^2 w}{\partial x \partial y}\ , \qquad \kappa_{xy} = -\frac{1}{2}\frac{\partial^2 w}{\partial x^2}\ , \qquad \kappa_{yx} = \frac{1}{2}\frac{\partial^2 w}{\partial y^2}\ . \tag{14}$$

The strain energy density in the case of a linear and isotropic material response takes the following form

$$W = 2\mu\Big(\varepsilon_{xz}^2 + \varepsilon_{yz}^2\Big) + 2\big(\eta + \eta'\big)\Big(\kappa_{xx}^2 + \kappa_{yy}^2\Big) + 2\eta\Big(\kappa_{xy}^2 + \kappa_{yx}^2\Big) + 4\eta'\kappa_{xy}\kappa_{yx}\,, \tag{15}$$

where μ has the same meaning as the shear modulus in the classical theory, and $\big(\eta, \eta'\big)$ are the couple-stress moduli with dimensions of force. The elastic moduli must satisfy the following inequalities so that the strain energy density is positive definite

$$\mu > 0\ , \qquad \eta > 0\ , \qquad -1 < \beta = \eta'\big/\eta < 1\ . \tag{16}$$

Further, the stress and couple-stress components are written in terms of the displacement field as

$$\begin{aligned} \sigma_{xz} &= \mu\frac{\partial}{\partial x}\Big(w - \ell^2\nabla^2 w\Big)\,, \qquad \sigma_{zx} = \mu\frac{\partial}{\partial x}\Big(w + \ell^2\nabla^2 w\Big), \\ \sigma_{yz} &= \mu\frac{\partial}{\partial y}\Big(w - \ell^2\nabla^2 w\Big)\,, \qquad \sigma_{zy} = \mu\frac{\partial}{\partial y}\Big(w + \ell^2\nabla^2 w\Big), \end{aligned} \tag{17}$$

$$
\begin{aligned}
m_{xx} &= 4\big(\eta+\eta'\big)\kappa_{xx} = 2\big(\eta+\eta'\big)\frac{\partial^2 w}{\partial x\partial y},\\
m_{yy} &= 4\big(\eta+\eta'\big)\kappa_{yy} = -2\big(\eta+\eta'\big)\frac{\partial^2 w}{\partial x\partial y} = -m_{xx},\\
m_{xy} &= 4\eta\kappa_{xy} + 4\eta'\kappa_{yx} = -2\eta\frac{\partial^2 w}{\partial x^2} + 2\eta'\frac{\partial^2 w}{\partial y^2},\\
m_{yx} &= 4\eta\kappa_{yx} + 4\eta'\kappa_{xy} = 2\eta\frac{\partial^2 w}{\partial y^2} - 2\eta'\frac{\partial^2 w}{\partial x^2}\ ,
\end{aligned}
\tag{18}
$$

with $\ell = \big(\eta/\mu\big)^{1/2}$ being the characteristic material length of isotropic couple-stress elasticity.

We also cite at this point the pertinent tractions that can be prescribed on a surface defined by the unit normal $\mathbf{n} = \big(0, \pm 1\big)$ (Mindlin and Tiersten, 1962)

$$
P_z^{(n)} \equiv t_{yz} = \sigma_{yz} + \frac{1}{2}\frac{\partial m_{yy}}{\partial x}, \qquad R_x^{(n)} = m_{yx}\ , \tag{19}
$$

where t_{yz} denotes the total shear stress. These expressions will be useful in the formulation of the antiplane crack problem.

Finally, combining Eqs. (12)-(18), a scalar equilibrium equation is obtained in terms of the out-of-plane displacement

$$
\nabla^2 w - \ell^2 \nabla^4 w = 0\ . \tag{20}
$$

3. Dislocation dipoles in couple-stress elasticity

In this section, the stress fields of plane dislocation dipoles in couple-stress elasticity are derived. As shown in Fig. 2, the three types of translational dislocations (climb, glide, and screw) may be combined to create pairs of equal and opposite sign dislocations, which leads to three cases of horizontal and three types of vertical dislocation dipoles. The product of the dislocation Burgers vector and the separation distance w_d of the pair is termed strength or intensity of the dipole. The intensity (or strength) of a dipole is usually denoted by b_{ij}, where i denotes the direction of the Burgers vector of the two dislocations and j denotes the normal direction to the

segment w_d that separates the dislocation pair. Cases (a) and (d) correspond to opening type of displacement discontinuity, cases (b) and (e) to tangential displacement discontinuity, and cases (c) and (f) to antiplane deformation.

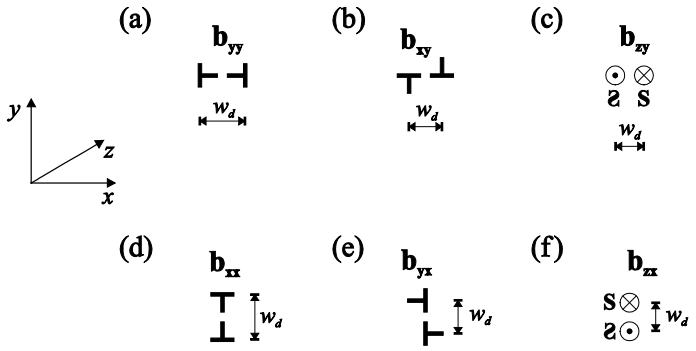

Fig. 2: Horizontal and vertical dislocation dipoles.

Dislocation dipoles can be distinguished to *infinitesimal* and *finite* based on the separation distance w_d (Kroupa, 1965). The stress field of a finite dislocation dipole is derived by superposing the corresponding fields of the two discrete dislocations that form the pair. For instance, the normal stress component $\sigma_{yy}^{(b_{yy})}$ of a finite climb dislocation dipole (Fig. 2a) placed at the origin of a Cartesian coordinate system is obtained in classical elasticity as (Hills et al., 1996)

$$\sigma_{yy}^{(b_{yy})}\left(x,\,0\right)=\sigma_{yy}^{b_y^{(1)}}\left(x-w_d/2,\,0\right)+\sigma_{yy}^{b_y^{(2)}}\left(x+w_d/2,\,0\right)= \\ -\frac{\mu\left|b_y\right|}{2\pi\left(1-\nu\right)\left(x-w_d/2\right)}+\frac{\mu\left|b_y\right|}{2\pi\left(1-\nu\right)\left(x+w_d/2\right)}=\frac{2\mu\left|b_y\right|w_d}{\pi\left(1-\nu\right)\left(4x^2-w_d^2\right)}\,, \tag{21}$$

where $b_y^{(i)}$ are the two discrete climb dislocations that form the dipole.

In the case of an infinitesimal dislocation dipole, it is required that $w_d\to 0$ and $b\to\infty$ while the quantity $w_d\,b$ is finite, so that Eq. (21) is written as

$$\sigma_{yy}\left(x,0\right)=\frac{\mu\left|b_y\right|w_d}{2\pi\left(1-\nu\right)x^2}\ . \tag{22}$$

Essentially, the stress field of an infinitesimal dislocation dipole may be derived by differentiating the field of the constituent discrete dislocations (in this case climb). From Eq. (22), it is obvious that the stress field reduces faster with respect to the distance compared to that of a discrete dislocation. The elastic energy of dipoles is significantly lower than that of discrete defects and therefore they are met in large quantities. Further details regarding the geometry and the nucleation method of dislocation dipoles may be found indicatively in the works of Tetelman (1962), Gilman (1964) and Kroupa (1966).

Following the procedure described above, we evaluate the stress fields of *infinitesimal* dislocation dipoles which will serve as influence functions in the crack problems under consideration. The stress and couple-stress fields of a *climb* dislocation dipole are derived using the expressions for a discrete climb dislocation in couple stress elasticity (Baxevanakis et al., 2017a) as

$$\begin{aligned}\sigma_{xx}^{\left(b_{yy}\right)}&=\frac{\mu b_y w_d}{2\pi\left(1-\nu\right)r^2}\cos 4\theta-\frac{6\mu b_y w_d}{\pi r^2}\left[\frac{2\ell^2}{r^2}-K_2\left(\frac{r}{\ell}\right)\right]\cos 4\theta\\&-\frac{\mu b_y w_d}{4\pi\ell^2}\left\{K_0\left(\frac{r}{\ell}\right)+\left[3K_0\left(\frac{r}{\ell}\right)-4K_2\left(\frac{r}{\ell}\right)\right]\cos 4\theta\right\},\end{aligned} \tag{23}$$

$$\begin{aligned}\sigma_{yy}^{\left(b_{yy}\right)}&=\frac{\mu b_y w_d}{2\pi\left(1-\nu\right)r^2}\left(2\cos 2\theta-\cos 4\theta\right)+\frac{6\mu b_y w_d}{\pi r^2}\left[\frac{2\ell^2}{r^2}-K_2\left(\frac{r}{\ell}\right)\right]\cos 4\theta\\&+\frac{\mu b_y w_d}{4\pi\ell^2}\left\{K_0\left(\frac{r}{\ell}\right)+\left[3K_0\left(\frac{r}{\ell}\right)-4K_2\left(\frac{r}{\ell}\right)\right]\cos 4\theta\right\},\end{aligned} \tag{24}$$

$$\begin{aligned}\sigma_{xy}^{\left(b_{yy}\right)}&=-\frac{\mu b_y w_d}{2\pi\left(1-\nu\right)r^2}\left(\sin 2\theta-\sin 4\theta\right)-\frac{6\mu b_y w_d}{\pi r^2}\left[\frac{2\ell^2}{r^2}-K_2\left(\frac{r}{\ell}\right)\right]\sin 4\theta\\&-\frac{\mu b_y w_d}{4\pi\ell^2}\left\{2K_0\left(\frac{r}{\ell}\right)\sin 2\theta+\left[3K_0\left(\frac{r}{\ell}\right)-4K_2\left(\frac{r}{\ell}\right)\right]\sin 4\theta\right\},\end{aligned} \tag{25}$$

$$\begin{aligned}\sigma_{yx}^{\left(b_{yy}\right)}&=-\frac{\mu b_y w_d}{2\pi\left(1-\nu\right)r^2}\left(\sin 2\theta-\sin 4\theta\right)-\frac{6\mu b_y w_d}{\pi r^2}\left[\frac{2\ell^2}{r^2}-K_2\left(\frac{r}{\ell}\right)\right]\sin 4\theta\\&+\frac{\mu b_y w_d}{4\pi\ell^2}\left\{2K_0\left(\frac{r}{\ell}\right)\sin 2\theta-\left[3K_0\left(\frac{r}{\ell}\right)-4K_2\left(\frac{r}{\ell}\right)\right]\sin 4\theta\right\},\end{aligned} \tag{26}$$

$$
\begin{aligned}
m_{xz}^{(b_{yy})} &= -\frac{\mu b_y w_d}{4\pi\ell^2} r\left[K_2\left(\frac{r}{\ell}\right) - K_0\left(\frac{r}{\ell}\right)\right](\sin\theta - \sin 3\theta) \\
&\quad + \frac{2\mu b_y w_d}{\pi r}\left[\frac{2\ell^2}{r^2} - K_2\left(\frac{r}{\ell}\right)\right]\sin 3\theta \ ,
\end{aligned}
\tag{27}
$$

$$
\begin{aligned}
m_{yz}^{(b_{yy})} &= -\frac{\mu b_y w_d}{4\pi\ell^2} r\left[K_2\left(\frac{r}{\ell}\right) - K_0\left(\frac{r}{\ell}\right)\right](\cos\theta - \cos 3\theta) \\
&\quad - \frac{2\mu b_y w_d}{\pi r}\left[\frac{2\ell^2}{r^2} - K_2\left(\frac{r}{\ell}\right)\right]\cos 3\theta \ .
\end{aligned}
\tag{28}
$$

Employing the asymptotic relations of the modified Bessel functions (Eq. (46)), we observe that as $r \to 0$, the stresses σ_{pq} exhibit a quadratic singularity that arises also in classical elasticity. On the other hand, both couple-stress m_{qz} have a Cauchy type singularity. The stress field reduces to the corresponding solution of classical elasticity as $\ell \to 0$ (Weertman, 1996).

The full-field solution for a *glide* dislocation dipole is obtained using the expressions for a discrete glide dislocation in couple stress elasticity (Baxevanakis et al., 2017b)

$$
\begin{aligned}
\sigma_{xx}^{(b_{xy})} &= -\frac{\mu b_x w_d}{2\pi\left(1-\nu\right) r^2}(\sin 2\theta + \sin 4\theta) + \frac{6\mu b_x w_d}{\pi r^2}\left[\frac{2\ell^2}{r^2} - K_2\left(\frac{r}{\ell}\right)\right]\sin 4\theta \\
&\quad - \frac{\mu b_x w_d}{4\pi\ell^2}\left\{2K_0\left(\frac{r}{\ell}\right)\sin 2\theta - \left[3K_0\left(\frac{r}{\ell}\right) - 4K_2\left(\frac{r}{\ell}\right)\right]\sin 4\theta\right\} \ ,
\end{aligned}
\tag{29}
$$

$$
\begin{aligned}
\sigma_{yy}^{(b_{xy})} &= -\frac{\mu b_x w_d}{2\pi\left(1-\nu\right) r^2}(\sin 2\theta - \sin 4\theta) - \frac{6\mu b_x w_d}{\pi r^2}\left[\frac{2\ell^2}{r^2} - K_2\left(\frac{r}{\ell}\right)\right]\sin 4\theta \\
&\quad + \frac{\mu b_x w_d}{4\pi\ell^2}\left\{2K_0\left(\frac{r}{\ell}\right)\sin 2\theta - \left[3K_0\left(\frac{r}{\ell}\right) - 4K_2\left(\frac{r}{\ell}\right)\right]\sin 4\theta\right\} \ ,
\end{aligned}
\tag{30}
$$

$$
\begin{aligned}
\sigma_{xy}^{(b_{xy})} &= \frac{\mu b_x w_d}{2\pi\left(1-\nu\right) r^2}\cos 4\theta - \frac{6\mu b_x w_d}{\pi r^2}\left[\frac{2\ell^2}{r^2} - K_2\left(\frac{r}{\ell}\right)\right]\cos 4\theta \\
&\quad - \frac{\mu b_x w_d}{4\pi\ell^2}\left\{K_0\left(\frac{r}{\ell}\right) + \left[3K_0\left(\frac{r}{\ell}\right) - 4K_2\left(\frac{r}{\ell}\right)\right]\cos 4\theta\right\} \ ,
\end{aligned}
\tag{31}
$$

$$
\begin{aligned}
\sigma_{yx}^{(b_{xy})} &= \frac{\mu b_x w_d}{2\pi\left(1-\nu\right) r^2}\cos 4\theta - \frac{6\mu b_x w_d}{\pi r^2}\left[\frac{2\ell^2}{r^2} - K_2\left(\frac{r}{\ell}\right)\right]\cos 4\theta \\
&\quad + \frac{\mu b_x w_d}{4\pi\ell^2}\left[3K_0\left(\frac{r}{\ell}\right)\left(1 - \cos 4\theta\right) + 4K_2\left(\frac{r}{\ell}\right)\left(\cos 2\theta + \cos 4\theta\right)\right] \ ,
\end{aligned}
\tag{32}
$$

$$m_{xz}^{(b_{xy})} = -\frac{\mu b_x w_d}{4\pi\ell^2} r\left[K_2\left(\frac{r}{\ell}\right) - K_0\left(\frac{r}{\ell}\right)\right](3\cos\theta + \cos 3\theta) + \frac{2\mu b_x w_d}{\pi r}\left[\frac{2\ell^2}{r^2} - K_2\left(\frac{r}{\ell}\right)\right]\cos 3\theta \ , \tag{33}$$

$$m_{yz}^{(b_{xy})} = -\frac{\mu b_x w_d}{4\pi\ell^2} r\left[K_2\left(\frac{r}{\ell}\right) - K_0\left(\frac{r}{\ell}\right)\right](\sin\theta + \sin 3\theta) + \frac{2\mu b_x w_d}{\pi r}\left[\frac{2\ell^2}{r^2} - K_2\left(\frac{r}{\ell}\right)\right]\sin 3\theta \ . \tag{34}$$

Asymptotic analysis shows that as $r \to 0$, the stresses σ_{pq} retain the quadratic singularity observed in classical elasticity while the couple-stresses m_{qz} have a Cauchy type singularity. For $\ell \to 0$, the classical elasticity solution is recovered.

Accordingly, the stress and couple-stress expressions of a *screw* dislocation dipole are derived using the relations for a discrete screw dislocation in couple stress elasticity (Baxevanakis et al., 2017b)

$$\sigma_{xz}^{(b_{zy})} = -\frac{\mu b_z w_d}{2\pi r^2}\sin 2\theta + \frac{3\mu b_z \ell^2 w_d\left(1+\beta\right)}{\pi r^4}\sin 4\theta \ , \tag{35}$$

$$\sigma_{yz}^{(b_{zy})} = \frac{\mu b_z w_d}{2\pi r^2}\cos 2\theta - \frac{3\mu b_z \ell^2 w_d\left(1+\beta\right)}{\pi r^4}\cos 4\theta \ , \tag{36}$$

$$m_{yy}^{(b_{zy})} = -m_{xx}^{(b_{zy})} = \frac{2\mu b_z \ell^2 w_d\left(1+\beta\right)}{\pi r^3}\cos 3\theta - \frac{12\mu b_z \ell^2 w_d\left(1+\beta\right)^2}{\pi r^3}\left[\frac{2\ell^2}{r^2} - K_2\left(\frac{r}{\ell}\right)\right] \times\cos 5\theta + \frac{\mu b_z w_d\left(1+\beta\right)^2}{4\pi r}\left\{K_2\left(\frac{r}{\ell}\right)\cos 3\theta - \left[6K_0\left(\frac{r}{\ell}\right) - 9K_2\left(\frac{r}{\ell}\right)\right]\cos 5\theta\right\} + \frac{\mu b_z w_d\left(1+\beta\right)^2}{32\pi\ell^2} r\left[K_0\left(\frac{r}{\ell}\right) - K_2\left(\frac{r}{\ell}\right)\right]\left(2\cos\theta - \cos 3\theta - \cos 5\theta\right) \ , \tag{37}$$

$$
\begin{aligned}
m_{yx}^{(b_{zy})} = & -\frac{2\mu b_z \ell^2 w_d \left(1+\beta\right)}{\pi r^3}\sin 3\theta + \frac{12\mu b_z \ell^2 w_d \left(1+\beta\right)^2}{\pi r^3}\left[\frac{2\ell^2}{r^2} - K_2\left(\frac{r}{\ell}\right)\right]\sin 5\theta \\
& + \frac{3\mu b_z w_d \left(1+\beta\right)^2}{4\pi r}\left[2K_0\left(\frac{r}{\ell}\right) - 3K_2\left(\frac{r}{\ell}\right)\right]\sin 5\theta + \frac{\mu b_z w_d \left(1+\beta\right)\left(1-3\beta\right)}{4\pi r} \\
& \times K_2\left(\frac{r}{\ell}\right)\sin 3\theta - \frac{\mu b_z w_d \left(1-\beta^2\right)}{16\pi\ell^2} r\left[K_0\left(\frac{r}{\ell}\right) - K_2\left(\frac{r}{\ell}\right)\right]\left(\sin\theta + \sin 3\theta\right) \\
& + \frac{\mu b_z w_d \left(1+\beta\right)^2}{32\pi\ell^2} r\left[K_0\left(\frac{r}{\ell}\right) - K_2\left(\frac{r}{\ell}\right)\right]\left(\sin 3\theta + \sin 5\theta\right),
\end{aligned}
\tag{38}
$$

$$
\begin{aligned}
m_{xy}^{(b_{zy})} = & -\frac{2\mu b_z \ell^2 w_d \left(1+\beta\right)}{\pi r^3}\sin 3\theta + \frac{12\mu b_z \ell^2 w_d \left(1+\beta\right)^2}{\pi r^3}\left[\frac{2\ell^2}{r^2} - K_2\left(\frac{r}{\ell}\right)\right]\sin 5\theta \\
& + \frac{3\mu b_z w_d \left(1+\beta\right)^2}{4\pi r}\left[2K_0\left(\frac{r}{\ell}\right) - 3K_2\left(\frac{r}{\ell}\right)\right]\sin 5\theta - \frac{\mu b_z w_d \left(1+\beta\right)\left(3-\beta\right)}{4\pi r} \\
& \times K_2\left(\frac{r}{\ell}\right)\sin 3\theta + \frac{\mu b_z w_d \left(1-\beta^2\right)}{16\pi\ell^2} r\left[K_0\left(\frac{r}{\ell}\right) - K_2\left(\frac{r}{\ell}\right)\right]\left(\sin\theta + \sin 3\theta\right) \\
& + \frac{\mu b_z w_d \left(1+\beta\right)^2}{32\pi\ell^2} r\left[K_0\left(\frac{r}{\ell}\right) - K_2\left(\frac{r}{\ell}\right)\right]\left(\sin 3\theta + \sin 5\theta\right).
\end{aligned}
\tag{39}
$$

Based on the asymptotic behavior of the modified Bessel functions we conclude that the shear stresses exhibit an r^{-4} singularity, whereas the couple-stresses behave as r^{-3} at the dislocation core. Also, the classical elasticity solution is obtained for $\beta \to -1$, i.e. $\eta = -\eta'$.

4. Formulation of the crack problems and influence functions

In this section we formulate the interaction problems of a finite-length crack with plane and antiplane defects. In all cases, we consider a straight crack of finite-length $2a$ in an infinite elastic microstructured domain characterized by couple-stress elasticity theory. The crack interacts with a horizontal climb (b_{yy}), glide (b_{xy}), or screw (b_{zy}) dislocation dipole (as defined in Fig. 2) lying at the crack plane ($y = 0$) at a distance d from the crack center, as shown in Fig. 3. Plane strain conditions prevail in the first two cases and antiplane strain in the latter one while there is no other loading applied in the body. The crack faces are described by the outward normal unit vector $\mathbf{n} = \left(0, \pm 1\right)$ and are assumed to be traction-free.

The solution procedure consists of decomposing the main crack problem to two auxiliary problems and superposing their solutions. In the first auxiliary problem, an *uncracked* domain subjected to the loading of a horizontal (climb, glide, or screw) dislocation dipole that lies along the crack line at a distance d from the crack center is considered. In the second auxiliary problem (usually referred to as corrective solution), a geometrically identical body to the initial *cracked* one without the dislocation dipole is studied. In this case, the only loading is applied along the crack faces and consists of equal and opposite tractions to those generated in the first auxiliary problem.

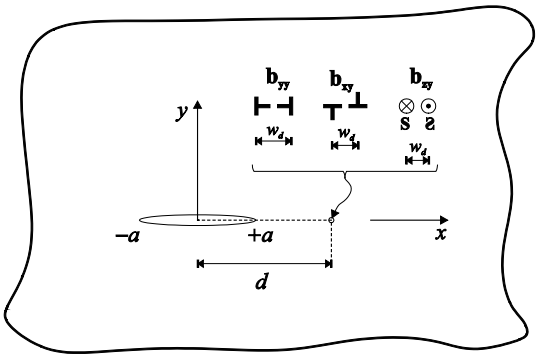

Fig. 3: Interaction of a finite-length plane crack with a horizontal climb, glide, or screw dipole.

4.1 Interaction of a finite-length crack with a climb dislocation dipole

The boundary conditions along the crack faces for the opening mode problem have the following form

$$\sigma_{yx}\Big(x,\,0\Big)=0\;,\qquad \sigma_{yy}\Big(x,\,0\Big)=0\;,\qquad m_{yz}=0\;,\qquad \text{for}\qquad \Big|x\Big|<a\;. \tag{40}$$

Further, the regularity conditions at infinity are

$$\sigma^{\infty}_{pq}\to 0\;,\qquad m^{\infty}_{qz}\to 0\qquad \text{as}\qquad r\to\infty\,, \tag{41}$$

where $\Big(p,q\Big)=\Big(x,y\Big)$ and $r=\Big(x^2+y^2\Big)^{1/2}$ is the distance from the origin. Eq. (41) suggests that the only loading induced in the problem is that of the climb dislocation dipole.

According to Eqs. (24) and (28), a climb dislocation dipole (either infinitesimal or finite) in an infinite isotropic couple-stress medium induces both normal stresses $\sigma_{yy}^{\left(b_{yy}\right)}\left(x,0\right)$ and couple-stresses $m_{yz}^{\left(b_{yy}\right)}\left(x,0\right)$ along the slip plane ($y=0$). On the other hand, there are no shear stresses produced by this defect at the slip plane, so that $\sigma_{yx}^{\left(b_{yy}\right)}\left(x,0\right)=0$.

Now, the boundary conditions of the corrective solution along the crack faces take the following form

$$\begin{aligned} &\sigma_{yy}\left(x,\,0\right)=-\sigma_{yy}^{\left(b_{yy}\right)}\left(x-d,\,0\right), \qquad \sigma_{yx}\left(x,\,0\right)=0\,, \\ &m_{yz}\left(x,\,0\right)=-m_{yz}^{\left(b_{yy}\right)}\left(x-d,\,0\right), \qquad \text{for} \quad \left|x\right|<a\,, \end{aligned} \tag{42}$$

augmented with the regularity conditions (41). The same problem in the context of classical isotropic elasticity theory is described by the first two conditions of Eq. (42) only. To solve that problem, a distribution of infinitesimal horizontal climb dislocation dipoles would be sufficient (Hills et al., 1996). However, as discussed in Baxevanakis et al. (2017a), in couple-stress theory it is not possible to satisfy simultaneously all three boundary conditions of Eq. (42) by a distribution of a single nucleus of strain (either discrete dislocations or dislocation dipoles) only. In fact, it is necessary to distribute along the crack faces not only discontinuities in the displacement u_y (i.e. infinitesimal climb dislocation dipoles) but also discontinuities in the rotation vector. In light of the above considerations, we introduce the *infinitesimal 'constrained' wedge disclination dipole* (Ω_{zy}) as the necessary rotational defect that needs to be distributed along the crack faces so that the boundary conditions of the problem are satisfied. This defect consists of two opposite sign constrained wedge disclinations with the distance between them approaching zero (details about the derivation of its full-field solution are provided in Appendix A). Then, the influence functions of the crack problem are obtained from the superposition of the stress and couple-stress fields of the translational and rotational defects described above (Eqs. (A2) and (A6), Appendix A). These are expressed as

$$\sigma_{yy}\left(x,\,0\right)=\sigma_{yy}^{\left(b_{yy}\right)}\left(x,0\right)+\sigma_{yy}^{\left(\Omega_{zy}\right)}\left(x,0\right), \quad m_{yz}\left(x,\,0\right)=m_{yz}^{\left(b_{yy}\right)}\left(x,0\right)+m_{yz}^{\left(\Omega_{zy}\right)}\left(x,0\right), \tag{43}$$

where

$$\begin{aligned}
&\sigma_{yy}^{\left(b_{yy}\right)}\left(x,0\right)=b_y w_d\left[L_{11}\left(x\right)+\left(L_{22}\left(x\right)\Big/\ell^2\right)\right], \qquad && \sigma_{yy}^{\left(\Omega_{zy}\right)}\left(x,0\right)=\Omega_z w_d L_{12}\left(x\right),\\
&m_{yz}^{\left(b_{yy}\right)}\left(x,0\right)=b_y w_d L_{12}\left(x\right), && m_{yz}^{\left(\Omega_{zy}\right)}\left(x,0\right)=\Omega_z w_d L_{22}\left(x\right),
\end{aligned} \tag{44}$$

and

$$\begin{aligned}
&L_{11}\left(x\right)=\frac{\mu}{2\pi\left(1-\nu\right)x^2}+\frac{6\mu}{\pi x^2}\left[\frac{2\ell^2}{x^2}-K_2\left(\frac{\left|x\right|}{\ell}\right)\right], \qquad L_{12}\left(x\right)=\frac{2\mu}{\pi x}\left[K_2\left(\frac{\left|x\right|}{\ell}\right)-\frac{2\ell^2}{x^2}\right],\\
&L_{22}\left(x\right)=\frac{\mu}{\pi}\left[K_0\left(\frac{\left|x\right|}{\ell}\right)-K_2\left(\frac{\left|x\right|}{\ell}\right)\right],
\end{aligned} \tag{45}$$

where $K_i\left(\left|x\right|\Big/\ell\right)$ is the i^{th} order modified Bessel function of the second kind.

The following points are of notice regarding the characteristics of the stress field described in Eqs. (43)-(45):

(i) As $x\to 0$, the asymptotic relations below are derived for expressions involving the modified Bessel functions

$$\begin{aligned}
&\frac{1}{x}\left[\frac{2\ell^2}{x^2}-K_2\left(\frac{\left|x\right|}{\ell}\right)\right]=O\left(\left(2x\right)^{-1}\right), \qquad && \frac{1}{x^2}\left[\frac{2\ell^2}{x^2}-K_2\left(\frac{\left|x\right|}{\ell}\right)\right]=O\left(\left(2x\right)^{-2}\right),\\
&\left[K_0\left(\frac{\left|x\right|}{\ell}\right)-K_2\left(\frac{\left|x\right|}{\ell}\right)\right]=O\left(\left(-2x\right)^{-2}-\ln\left|x\right|\right).
\end{aligned} \tag{46}$$

Based on these relations, it can be deduced that as $x\to 0$, the normal stress σ_{yy} (Eq. $(43)_1$) exhibits a *quadratic* and a *logarithmic* singularity due to the climb dislocation dipole and a *Cauchy* type singularity due to the constrained wedge disclination dipole. On the contrary, the couple-stress m_{yz} (Eq. $(43)_2$) has a *quadratic* and a *logarithmic* singularity due to the constrained wedge disclination dipole and a *Cauchy* type singularity due to the climb dislocation dipole.

(ii) As $x\to\pm\infty$, it may be shown that both $\sigma_{yy}\to 0$ and $m_{yz}\to 0$. Therefore, the constrained wedge disclination dipole does not induce normal stresses at infinity.

(iii) As $\ell\to 0$, the couple-stress m_{yz} vanishes. Thus, the constrained wedge disclination dipole induces stresses and couple-stresses only for $\ell\neq 0$, i.e. when the material microstructure is

considered. On the other hand, as $\ell \to 0$, the normal stress σ_{yy} reduces to the expression $\sigma_{yy}^{(b_{yy})} = \mu b_y w_d \big/ 2\pi\big(1-\nu\big)x^2$, which is the influence function for the opening mode problem in classical elasticity, when dislocation dipoles are used in the formulation.

4.2 Interaction of a finite-length crack with a glide dislocation dipole

The boundary conditions that describe the plane shear problem are given in Eq. (40) accompanied by the regularity conditions (41). According to the full field solution of a glide dislocation dipole (Eqs. (29)-(34)), it is observed that for $y = 0$ this defect induces only shear stresses $\sigma_{yx}^{(b_{xy})}\big(x,0\big)$ along the crack faces, so that $\sigma_{yy}^{(b_{xy})}\big(x,0\big) = 0$ and $m_{yz}^{(b_{xy})}\big(x,0\big) = 0$.

An analogous procedure to the one described in the previous section is followed to obtain a solution for this crack problem. We first consider an *uncracked* medium subjected to the loading $\sigma_{yx}^{(b_{xy})}\big(x-d,0\big)$ of a horizontal glide dislocation dipole that lies along the crack line at a distance d from the crack center. The solution to this problem is obtained based on Eqs. (29)-(34) in the case of an infinitesimal defect or by following the procedure described in Eq. (21) in the case of a finite dislocation dipole. Accordingly, the boundary conditions of the second auxiliary problem read as

$$\begin{aligned} &\sigma_{yy}\big(x,\,0\big) = 0\ , \qquad \sigma_{yx}\big(x,\,0\big) = -\sigma_{yx}^{(b_{xy})}\big(x-d,\,0\big)\ , \\ &m_{yz}\big(x,\,0\big) = 0\ , \qquad \text{for} \quad \big|x\big| < a\ , \end{aligned} \tag{47}$$

augmented with the regularity conditions (41). The boundary conditions in Eq. (47) are satisfied by a distribution of infinitesimal horizontal glide dislocation dipoles along the crack faces, contrary to the opening mode problem discussed earlier. It is also noted that Eq. $(47)_1$ and $(47)_3$ are automatically satisfied since this strain nucleus does not generate any normal stresses or couple-stresses along the crack plane (see Eqs. (30) and (34)). In the context of isotropic classical elasticity, the same problem is governed by the first and second conditions of Eq. (47), which are also satisfied by a distribution of infinitesimal horizontal glide dislocation dipoles along

the crack faces. In that case, the interaction problem is described by a hyper-singular integral equation with quadratic singularity.

Finally, from Eqs. (30), (32), and (34), we obtain the following relations for $y = 0$

$$\sigma_{yx}^{(b_{xy})}\Big(x,\,0\Big) = \frac{\mu b_{x} w_{d}}{2\pi\Big(1-\nu\Big)x^{2}} - \frac{6\mu b_{x} w_{d}}{\pi x^{2}}\left[\frac{2\ell^{2}}{x^{2}} - K_{2}\left(\frac{\Big|x\Big|}{\ell}\right)\right] + \frac{2\mu b_{x} w_{d}}{\pi\ell^{2}}\,K_{2}\left(\frac{\Big|x\Big|}{\ell}\right)\,, \tag{48}$$

$$\sigma_{yy}^{(b_{xy})}\Big(x,\,0\Big) = 0\,, \qquad m_{yz}^{(b_{xy})}\Big(x,\,0\Big) = 0\,. \tag{49}$$

Eq. (48) is the influence function for the plane shear mode problem in couple-stress elasticity in a displacement-based formulation context.

4.3 Interaction of a finite-length crack with a screw dislocation dipole

The interaction problem of a finite-length crack and a screw dislocation dipole b_{zy} in couple-stress elasticity is studied next. Hence, the boundary conditions of this interaction problem are given in view of Eq. (19) as

$$t_{yz}\Big(x,\,0\Big) = \sigma_{yz}\Big(x,\,0\Big) + \frac{1}{2}\partial_{x} m_{yy}\Big(x,\,0\Big) = 0\,, \qquad m_{yx} = 0\,, \qquad \text{for} \qquad \Big|x\Big| < a\,, \tag{50}$$

along with the regularity conditions at infinity

$$\sigma_{pz}^{\infty} \to 0\,, \qquad m_{pq}^{\infty} \to 0 \qquad \text{as} \qquad r \to \infty\,, \tag{51}$$

where $\Big(p,q\Big) = \Big(x,y\Big)$ and $r = \Big(x^{2} + y^{2}\Big)^{1/2}$ is the distance from the origin.

The full field solution for an infinitesimal horizontal screw dislocation dipole (Eqs. (35)-(39)) shows that for $y = 0$ this defect generates shear stresses $\sigma_{yz}^{(b_{zy})}\Big(x,0\Big)$ and couple-stresses $m_{yy}^{(b_{zy})}\Big(x,0\Big)$ along the crack plane, while it holds that $m_{yx}^{(b_{zy})}\Big(x,0\Big) = 0$.

For the solution of the antiplane crack problem, we follow the decomposition in two auxiliary configurations introduced earlier in the plane crack problems: i) the uncracked geometrically identical to the initial body subjected to the loading $t_{yz}^{\left(b_{zy}\right)}\left(x-d,0\right)$ of a horizontal screw dislocation dipole placed at a distance d from the crack center along the crack plane, ii) the corrective solution problem described as

$$\begin{aligned} &t_{yz}\left(x,\,0\right)=-t_{yz}^{\left(b_{zy}\right)}\left(x-d,0\right)=-\sigma_{yz}^{\left(b_{zy}\right)}\left(x-d,\,0\right)-\frac{1}{2}\partial_x m_{yy}^{\left(b_{zy}\right)}\left(x-d,\,0\right),\\ &m_{yx}^{\left(b_{zy}\right)}\left(x,\,0\right)=0\,, \qquad\qquad \text{for } \left|x\right|<a\,, \end{aligned} \tag{52}$$

supplemented by the regularity condition (51). These boundary conditions are satisfied by a distribution of infinitesimal horizontal screw dislocation dipoles along the crack faces. From Eq. (38), it is inferred that the couple stress $m_{yx}^{\left(b_{zy}\right)}$ vanishes at $y=0$, so that Eq. $(52)_2$ is automatically satisfied. Accordingly, the same problem is described in classical elasticity by Eq. $(52)_1$ which is satisfied by the distribution of infinitesimal horizontal screw dislocation dipoles along the crack faces. In that context, the interaction problem is described by a hyper-singular integral equation with quadratic singularity.

Finally, from Eqs. (36) and (37), the total shear stress for $y=0$ becomes

$$\begin{aligned} t_{yz}^{\left(b_{zy}\right)}\left(x,\,0\right)=\sigma_{yz}^{\left(b_{zy}\right)}\left(x,\,0\right)+\frac{1}{2}\partial_x m_{yy}^{\left(b_{zy}\right)}\left(x,\,0\right)=\frac{\mu b_z w_d}{2\pi x^2}-\frac{6\mu b_z w_d \ell^2\left(1+\beta\right)}{\pi x^4}\\ +\frac{30\mu b_z w_d \ell^2\left(1+\beta\right)^2}{\pi x^4}\left[\frac{2\ell^2}{x^4}-K_2\left(\frac{\left|x\right|}{\ell}\right)\right]-\frac{3\mu b_z w_d\left(1+\beta\right)^2}{4\pi x^2}\\ \times\left[9K_2\left(\frac{\left|x\right|}{\ell}\right)-5K_0\left(\frac{\left|x\right|}{\ell}\right)\right]-\frac{\mu b_z w_d\left(1+\beta\right)^2}{4\pi\ell^2}\left[K_2\left(\frac{\left|x\right|}{\ell}\right)-K_0\left(\frac{\left|x\right|}{\ell}\right)\right]. \end{aligned} \tag{53}$$

Eq. (53) is the influence function for the antiplane shear mode problem in couple-stress elasticity in a displacement-based formulation framework. The previous expression behaves as $O\left(x^{-4}\right)$ as $x\to 0$ while for $\beta=-1$ it reduces to the corresponding influence function of classical elasticity theory.

5. Integral equation approach

5.1 Interaction of a finite-length crack with a climb dislocation dipole

The corrective stresses (Eq. (42)) are developed by a continuous distribution of climb dislocation dipoles and constrained wedge disclination dipoles along the crack faces, as discussed in Section 4.1. The elastic field generated by this distribution is derived by integrating the influence functions of the problem (Eqs. (43)-(45)) along the crack faces. It is reminded that the boundary condition described in Eq. $(42)_2$ is automatically satisfied since none of the distributed defects induces shear stresses along the crack plane $y = 0$, as observed in Eq. (A3). On the other hand, the simultaneous satisfaction of the first and third conditions of Eq. (42) leads to a system of coupled integral equations. Using asymptotic analysis, the singular parts of the kernels are separated from the regular and we eventually obtain the following system of hyper-singular integral equations

$$
\begin{aligned}
-\sigma_{yy}^{\left(b_{yy}\right)}\left(x-d,\,0\right) = {} & \frac{\mu\left(3-2\nu\right)}{2\pi\left(1-\nu\right)}\,\text{F.P.}\int_{-a}^{a}\frac{B_I\left(t\right)}{\left(x-t\right)^2}dt-\frac{\mu}{\pi a}\int_{-a}^{a}\frac{W\left(t\right)}{x-t}dt \\
& -\frac{\mu}{4\pi\ell^2}\int_{-a}^{a}B_I\left(t\right)\ln\frac{\left|x-t\right|}{\ell}dt+\frac{\mu}{\pi}\int_{-a}^{a}B_I\left(t\right)R_1\left(x-t\right)dt \\
& +\frac{\mu}{\pi a}\int_{-a}^{a}W\left(t\right)R_2\left(x-t\right)dt\ , \qquad \left|x\right|<a\ ,
\end{aligned}
\tag{54}
$$

$$
\begin{aligned}
-m_{yz}^{\left(b_{yy}\right)}\left(x-d,\,0\right) = {} & -\frac{2\mu\ell^2}{\pi a}\,\text{F.P.}\int_{-a}^{a}\frac{W\left(t\right)}{\left(x-t\right)^2}dt-\frac{\mu}{\pi}\int_{-a}^{a}\frac{B_I\left(t\right)}{x-t}dt \\
& -\frac{\mu}{\pi a}\int_{-a}^{a}W\left(t\right)\ln\frac{\left|x-t\right|}{\ell}dt+\frac{\mu}{\pi}\int_{-a}^{a}B_I\left(t\right)R_2\left(x-t\right)dt \\
& +\frac{\mu}{\pi a}\int_{-a}^{a}W\left(t\right)R_3\left(x-t\right)dt\ , \qquad \left|x\right|<a\ ,
\end{aligned}
\tag{55}
$$

where the symbol $\text{F.P.}\int$ denotes a Hadamard finite-part integral (see e.g. Monegato (1994)). The densities of climb dislocation dipoles and constrained wedge disclination dipoles, $B_I\left(t\right)$ and $W\left(t\right)$, are defined as

$$B_I\left(t\right)=\frac{db_{yy}\left(t\right)}{dt}=\Delta u_y\left(x\right)\,,\qquad W\left(t\right)=-a\,\frac{d\Omega_{zy}\left(t\right)}{dt}=-a\Delta\omega\left(t\right)\,. \tag{56}$$

In these expressions, $\Delta u_y\left(x\right)$ is the relative opening displacement and $\Delta\omega\left(x\right)$ the relative rotation between the upper and lower crack faces respectively. Hence, the climb dislocation dipole density corresponds to the relative displacement and the constrained wedge disclination dipole density is equal to the relative rotation at any point of the crack faces. Further, the kernels $R_q\left(x-t\right)$, for $q=1,\,2,\,3$, are defined as

$$\begin{aligned}
R_1\left(x-t\right)&=\frac{6}{\left(x-t\right)^2}\left[\frac{2\ell^2}{\left(x-t\right)^2}-K_2\left(\frac{\left|x-t\right|}{\ell}\right)-\frac{1}{6}\right]\\
&\quad+\frac{1}{\ell^2}\left[K_0\left(\frac{\left|x-t\right|}{\ell}\right)-K_2\left(\frac{\left|x-t\right|}{\ell}\right)+\frac{1}{4}\ln\left(\frac{\left|x-t\right|}{\ell}\right)\right],\\
R_2\left(x-t\right)&=-\frac{1}{x-t}\left[\frac{4\ell^2}{\left(x-t\right)^2}-K_2\left(\frac{\left|x-t\right|}{\ell}\right)-1\right],\\
R_3\left(x-t\right)&=\frac{2\ell^2}{\left(x-t\right)^2}+K_0\left(\frac{\left|x-t\right|}{\ell}\right)-K_2\left(\frac{\left|x-t\right|}{\ell}\right)+\ln\left(\frac{\left|x-t\right|}{\ell}\right).
\end{aligned} \tag{57}$$

Employing the asymptotic relations of the modified Bessel functions (Eq. (46)), it may be shown that the kernels in Eq. (57) are regular as $x\to t$ and $\ell>0$.

Next, the unknown defect densities, $B_I\left(t\right)$ and $W\left(t\right)$, should be expressed in such a way to account for the asymptotic behavior of the displacement and the rotation at the crack-tips. In the framework of couple-stress elasticity, both the displacement u_y and the rotation ω behave as $r^{1/2}$ near the crack-tips, where r is the radial distance from the crack-tip (Huang et al., 1997). Therefore, the densities are expressed as the product of a regular and bounded function with a singular function as follows

$$B_I\left(\tilde{t}\,\right)=\sum_{n=0}^{\infty}b_nU_n\left(\tilde{t}\,\right)\left(1-\tilde{t}^{\,2}\right)^{1/2}\,,\qquad W\left(\tilde{t}\,\right)=\sum_{n=0}^{\infty}c_nU_n\left(\tilde{t}\,\right)\left(1-\tilde{t}^{\,2}\right)^{1/2}\,,\qquad \left|\tilde{t}\,\right|<1\,, \tag{58}$$

where $U_n\left(\tilde{t}\right)$ are the Chebyshev polynomials of the second kind, $\left(b_n,\, c_n\right)$ are unknown parameters and $\tilde{t} = t/a$. It is noted that in the formulation of crack problems based on infinitesimal dislocation dipoles (displacement-based), no extra closure conditions are required to ensure that the normal displacement and the rotation are single-valued, which is the case in the formulation based on discrete dislocations (Baxevanakis et al., 2017a, b). These conditions ensure that $\Delta u_y\left(a\right) = \Delta u_y\left(-a\right) = 0$ and $\Delta\omega\left(a\right) = \Delta\omega\left(-a\right) = 0$, i.e. that there is no remaining net dislocation along the crack length. In the current formulation, the two dislocations that form the dipole cancel each other out (self-annihilation) and therefore, closure conditions are redundant. Returning to the solution of the system of singular equations (54) and (55), after introducing the dimensionless quantities $\tilde{x} = x/a$, $\tilde{d} = d/a$ and performing an appropriate normalization in the interval $\left[-1,\, 1\right]$, we obtain

$$
\begin{aligned}
-\frac{\pi\sigma_{yy}^{\left(b_{yy}\right)}\left(a\tilde{x} - a\tilde{d},\, 0\right)}{\mu} &= \frac{\left(3-2\nu\right)}{2\left(1-\nu\right)}\sum_{n=0}^{\infty} b_n\ \text{F.P.}\int_{-1}^{1}\frac{U_n\left(\tilde{t}\right)\left(1-\tilde{t}^{\,2}\right)^{1/2}}{\left(\tilde{x}-\tilde{t}\right)^2}d\tilde{t} \\
-\sum_{n=0}^{\infty} c_n\int_{-1}^{1}\frac{U_n\left(\tilde{t}\right)\left(1-\tilde{t}^{\,2}\right)^{1/2}}{\tilde{x}-\tilde{t}}d\tilde{t} &- \frac{a^2}{4\ell^2}\sum_{n=0}^{\infty} b_n\int_{-1}^{1} U_n\left(\tilde{t}\right)\left(1-\tilde{t}^{\,2}\right)^{1/2}\ln\left(\frac{a}{\ell}\left|\tilde{x}-\tilde{t}\right|\right)d\tilde{t} \\
&+\sum_{n=0}^{\infty} b_n\, Q_n^{(1)}\left(\tilde{x}\right) + \sum_{n=0}^{\infty} c_n\, Q_n^{(2)}\left(\tilde{x}\right), \qquad \left|\tilde{x}\right| < 1\,,
\end{aligned}
\tag{59}
$$

$$
\begin{aligned}
-\frac{\pi m_{yz}^{\left(b_{yy}\right)}\left(\tilde{x} - \tilde{d},\, 0\right)}{\mu} &= -\frac{2\ell^2}{a^2}\sum_{n=0}^{\infty} c_n\ \text{F.P.}\int_{-1}^{1}\frac{U_n\left(\tilde{t}\right)\left(1-\tilde{t}^{\,2}\right)^{1/2}}{\left(\tilde{x}-\tilde{t}\right)^2}d\tilde{t} \\
-\sum_{n=0}^{\infty} b_n\int_{-1}^{1}\frac{U_n\left(\tilde{t}\right)\left(1-\tilde{t}^{\,2}\right)^{1/2}}{\tilde{x}-\tilde{t}}d\tilde{t} &- \sum_{n=0}^{\infty} c_n\int_{-1}^{1} U_n\left(\tilde{t}\right)\left(1-\tilde{t}^{\,2}\right)^{1/2}\ln\left(\frac{a}{\ell}\left|\tilde{x}-\tilde{t}\right|\right)d\tilde{t} \\
&+\sum_{n=0}^{\infty} b_n\, Q_n^{(2)}\left(\tilde{x}\right) + \sum_{n=0}^{\infty} c_n\, Q_n^{(3)}\left(\tilde{x}\right), \qquad \left|\tilde{x}\right| < 1\,,
\end{aligned}
\tag{60}
$$

where the functions $Q_n^{(s)}\left(\tilde{x}\right)$ are defined as

$$Q_n^{(s)}\left(\tilde{x}\right) \equiv \int_{-1}^{1} U_n\left(\tilde{t}\right)\left(1-\tilde{t}^2\right)^{1/2} R_s\left(a\tilde{x}-a\tilde{t}\right) d\tilde{t} \;\;,\; s=1,\,2,\,3\,. \tag{61}$$

The integrals in Eq. (61) are regular and hence are evaluated numerically using the standard Gauss-Chebyshev quadrature whereas the hyper-singular, singular, and weakly singular (logarithmic) integrals in Eqs. (59) and (60) are calculated in closed form using Eqs. (B2), (B1), and (B5) in Appendix B. In view of this information, the system is written in discretized form as

$$\begin{aligned} -\frac{\sigma_{yy}^{\left(b_{yy}\right)}\left(a\tilde{x}-a\tilde{d},\,0\right)}{\mu} &= -\frac{\left(3-2\nu\right)}{2\left(1-\nu\right)}\sum_{n=0}^{\infty} b_n\left(n+1\right)U_n\left(\tilde{x}\right) - \sum_{n=0}^{\infty} c_n T_{n+1}\left(\tilde{x}\right) \\ &\quad -\frac{a^2}{4\ell^2}\left\{ b_0\left(\frac{1}{4}T_2\left(\tilde{x}\right)-\frac{1}{2}\ln 2\right) + \sum_{n=1}^{\infty} b_n\left[\frac{1}{2}\left(\frac{T_{n+2}\left(\tilde{x}\right)}{n+2}-\frac{T_n\left(\tilde{x}\right)}{n}\right)\right]\right\} \\ &\quad +\sum_{n=0}^{\infty} b_n Q_n^{(1)}\left(\tilde{x}\right) + \sum_{n=0}^{\infty} c_n\, Q_n^{(2)}\left(\tilde{x}\right), \qquad \left|\tilde{x}\right|<1\,, \end{aligned} \tag{62}$$

$$\begin{aligned} -\frac{m_{yz}^{\left(b_{yy}\right)}\left(\tilde{x}-\tilde{d},\,0\right)}{\mu} &= \frac{2\ell^2}{a^2}\sum_{n=0}^{\infty} c_n\left(n+1\right)U_n\left(\tilde{x}\right) - \sum_{n=0}^{\infty} b_n T_{n+1}\left(\tilde{x}\right) \\ &\quad -\left\{ c_0\left(\frac{1}{4}T_2\left(\tilde{x}\right)-\frac{1}{2}\ln 2\right) + \sum_{n=1}^{\infty} c_n\left[\frac{1}{2}\left(\frac{T_{n+2}\left(\tilde{x}\right)}{n+2}-\frac{T_n\left(\tilde{x}\right)}{n}\right)\right]\right\} \\ &\quad +\sum_{n=1}^{\infty} b_n\, Q_n^{(2)}\left(\tilde{x}\right) + \sum_{n=0}^{\infty} c_n\, Q_n^{(3)}\left(\tilde{x}\right), \qquad \left|\tilde{x}\right|<1\,. \end{aligned} \tag{63}$$

The system of Eqs. (62) and (63) is solved numerically by truncating the series at $n=N$ and using an appropriate collocation technique, where the collocation points are selected as the roots of the Chebyshev polynomial $T_{N+1}\left(\tilde{x}\right)$, viz. $\tilde{x}_k=\cos\left[\left(2k+1\right)\pi/2\left(N+1\right)\right]$ with $k=0,1,...,N$. Eqs. (62) and (63) form an algebraic system of $2N+2$ equations with $2N+2$ unknowns. It should be noted that the solution convergence is dependent on the ratio ℓ/a. Finally, after calculating the constants b_n and c_n $\left(n=0,...,N\right)$, the defect densities may be evaluated using Eq. (58).

5.2 Interaction of a finite-length crack with a glide dislocation dipole

Accordingly, in order to generate the corrective stresses (Eq. (47)) for the plane shear problem, it is necessary to distribute infinitesimal glide dislocation dipoles along the crack faces. The elastic field induced by the continuous distribution of these defects is derived by integrating the influence function of the problem (Eq. (48)) along the crack faces. Using asymptotic analysis to separate the singular from the regular part of the kernel, we derive the following expression

$$-\sigma_{yx}^{\left(b_{xy}\right)}\left(x-d,\,0\right)=\frac{\mu\left(3-2\nu\right)}{2\pi\left(1-\nu\right)}\,\text{F.P.}\int_{-a}^{a}\frac{B_{II}\left(t\right)}{\left(x-t\right)^{2}}dt-\frac{3\mu}{4\pi\ell^{2}}\int_{-a}^{a}B_{II}\left(t\right)\ln\frac{\left|x-t\right|}{\ell}dt \\ +\frac{\mu}{\pi}\int_{-a}^{a}B_{II}\left(t\right)R_{4}\left(x-t\right)dt\,,\qquad\left|x\right|<a\,, \tag{64}$$

where $B_{II}\left(t\right)=db_{xy}\left(t\right)\big/dt=\Delta u_{x}\left(t\right)$ is the glide dislocation dipole density at a point t $\left(\left|t\right|<a\right)$ and $\Delta u_{x}=u_{x}\left(t,\,0^{+}\right)-u_{x}\left(t,\,0^{-}\right)$ is the relative tangential displacement between the upper and lower crack faces. The regular kernel $R_{4}\left(x-t\right)$ is given as

$$R_{4}\left(x-t\right)=-\frac{2}{x-t}\left[\frac{6\ell^{2}}{\left(x-t\right)^{2}}-3K_{2}\left(\frac{\left|x-t\right|}{\ell}\right)+\frac{1}{2}\right]+\frac{1}{\ell^{2}}\left[2K_{2}\left(\frac{\left|x-t\right|}{\ell}\right)+\frac{3}{4}\ln\left(\frac{\left|x-t\right|}{\ell}\right)\right]. \tag{65}$$

Further, since the displacement u_{x} behaves as $r^{1/2}$ near the crack-tips in the context of couple-stress elasticity (Huang et al., 1997), the unknown density of glide dislocation dipoles, $B_{II}\left(t\right)$, may be written as

$$B_{II}\left(\tilde{t}\right)=\sum_{n=0}^{\infty}b_{n}U_{n}\left(\tilde{t}\right)\left(1-\tilde{t}^{2}\right)^{1/2}\,,\qquad\left|\tilde{t}\right|<1\,. \tag{66}$$

Then, the hyper-singular and weakly singular (logarithmic) integrals in Eq. (64) are evaluated in closed form employing Eqs. (B2) and (B5) in Appendix B while the regular integral is calculated numerically using the standard Gauss-Chebyshev quadrature. Based on the above

and after appropriate normalization in the interval $\left[-1,\,1\right]$, the integral equation (64) is expressed in the following discretized form

$$-\frac{\sigma_{yx}^{\left(b_{xy}\right)}\left(a\tilde{x}-a\tilde{d},\,0\right)}{\mu}=-\frac{\left(3-2\nu\right)}{2\left(1-\nu\right)}\sum_{n=0}^{\infty}b_n\left(n+1\right)U_n\left(\tilde{x}\right)-\frac{3a^2}{4\ell^2}\left\{b_0\left(\frac{1}{4}T_2\left(\tilde{x}\right)-\frac{1}{2}\ln 2\right)\right.$$
$$\left.+\sum_{n=1}^{\infty}b_n\left[\frac{1}{2}\left(\frac{T_{n+2}\left(\tilde{x}\right)}{n+2}-\frac{T_n\left(\tilde{x}\right)}{n}\right)\right]\right\}+\sum_{n=0}^{\infty}b_nQ_n^{(4)}\left(\tilde{x}\right),\qquad\left|\tilde{x}\right|<1\,. \tag{67}$$

where the function $Q_n^{(4)}\left(\tilde{x}\right)$ is defined as

$$Q_n^{(4)}\left(\tilde{x}\right)\equiv\int_{-1}^{1}U_n\left(\tilde{t}\right)\left(1-\tilde{t}^{\,2}\right)^{1/2}R_4\left(a\tilde{x}-a\tilde{t}\right)d\tilde{t}\,. \tag{68}$$

Eq. (67) forms an algebraic system of $N+1$ equations with $N+1$ unknowns that is solved numerically using the same collocation technique as in the opening mode problem (Section 5.1).

5.3 Interaction of a finite-length crack with a screw dislocation dipole

As in the previous crack problems, the corrective stresses (Eq. (52)) are generated by a continuous distribution of infinitesimal screw dislocation dipoles along the crack faces. The elastic field that is produced in this case is derived by integrating the influence function (Eq. (53)) along the crack faces. In view of the above, we obtain a hyper-singular integral equation with fourth order, quadratic, and logarithmic singularities that describes the crack problem. With the use of asymptotic analysis, we separate the singular from the regular part of the kernel and obtain the following governing equation of the crack problem

$$-t_{yz}^{(b_{zy})}\big(x-d,\,0\big)=-3c_1\ell^2\ \text{F.P.}\int_{-a}^{a}\frac{B_{III}\big(t\big)}{\big(x-t\big)^4}dt+c_2\,\text{F.P.}\int_{-a}^{a}\frac{B_{III}\big(t\big)}{\big(x-t\big)^2}dt$$
$$-\frac{\mu}{32\ell^2}\int_{-a}^{a}B_{III}\big(t\big)\ln\frac{\big|x-t\big|}{\ell}dt+c_3\int_{-a}^{a}B_{III}\big(t\big)R_5\big(x-t\big)dt\ ,\qquad \big|x\big|<a\ ,\tag{69}$$

where $B_{III}\big(t\big)=db_{zy}\big(t\big)\big/dt=\Delta w\big(t\big)$ is the screw dislocation dipole density at a point t $\big(\big|t\big|<a\big)$ and $\Delta w=w\big(t,\,0^+\big)-w\big(t,\,0^-\big)$ is the relative out-of-plane displacement between the upper and lower crack faces. The constants c_i, for $i=1,\,2,\,3$, are given as

$$c_1=\frac{\mu\big(1+\beta\big)\big(3-\beta\big)}{2\pi}\ ,\qquad c_2=\frac{\mu\big(\beta^2+2\beta+9\big)}{16\pi}\ ,\qquad c_3=\frac{\mu\big(1+\beta\big)^2}{\pi}\ ,\tag{70}$$

and the kernel $R_5\big(x-t\big)$ as

$$R_5\big(x-t\big)=-\frac{\ell^2}{\big(x-t\big)^4}\left\{30\left[K_2\left(\frac{\big|x-t\big|}{\ell}\right)-\frac{2\ell^2}{\big(x-t\big)^2}\right]+\frac{3}{2}\right\}+\frac{1}{8\big(x-t\big)^2}\left[30K_0\left(\frac{\big|x-t\big|}{\ell}\right)\right.$$
$$\left.-54K_2\left(\frac{\big|x-t\big|}{\ell}\right)-\frac{1}{2}\right]+\frac{1}{4\ell^2}\left[K_0\left(\frac{\big|x-t\big|}{\ell}\right)-K_2\left(\frac{\big|x-t\big|}{\ell}\right)+\frac{1}{8}\ln\left(\frac{\big|x-t\big|}{\ell}\right)\right].\tag{71}$$

Employing the asymptotic relations of the modified Bessel functions, it may be shown that the kernel $R_5\big(x-t\big)$ is regular as $x\to t$ in the closed interval $-a\le\big(x,\,t\big)\le a$. Also, it is noted that for $\beta=-1$, Eq. (69) reduces to the corresponding expression of classical elasticity.

Next, considering that the out-of-plane displacement w behaves as $r^{3/2}$ near the crack-tip region (Zhang et al., 1998), where r is the radial distance from the crack-tip, the unknown screw dislocation dipole density $B_{III}\big(t\big)$ may be written as

$$B_{III}\left(\tilde{t}\right)=\sum_{n=0}^{\infty}b_{n}U_{n}\left(\tilde{t}\right)\left(1-\tilde{t}^{2}\right)^{3/2}\ ,\qquad \left|\tilde{t}\right|<1\ . \tag{72}$$

As in the plane problems, it is reminded that no closure condition is required to ensure uniqueness of the values of the antiplane displacement for a closed loop around the crack.

After appropriate normalization over the interval $\left[-1,\,1\right]$, the integral equation (69) takes the following form for $\left|\tilde{x}\right|<1$

$$\begin{aligned}-t_{yz}^{\left(b_{zy}\right)}\left(a\tilde{x}-a\tilde{d},\,0\right)=&\\ -\frac{3c_{1}\ell^{2}}{a^{2}}\sum_{n=0}^{\infty}b_{n}\,\text{F.P.}\int_{-1}^{1}\frac{U_{n}\left(\tilde{t}\right)\left(1-\tilde{t}^{2}\right)^{3/2}}{\left(\tilde{x}-\tilde{t}\right)^{4}}d\tilde{t}\,+c_{2}\sum_{n=0}^{\infty}b_{n}\,\text{F.P.}\int_{-1}^{1}\frac{U_{n}\left(\tilde{t}\right)\left(1-\tilde{t}^{2}\right)^{3/2}}{\left(\tilde{x}-\tilde{t}\right)^{2}}d\tilde{t}&\\ -\frac{\mu a^{2}}{32\ell^{2}}\sum_{n=0}^{\infty}b_{n}\int_{-1}^{1}U_{n}\left(\tilde{t}\right)\left(1-\tilde{t}^{2}\right)^{3/2}\ln\left(\frac{a}{\ell}\left|\tilde{x}-\tilde{t}\right|\right)d\tilde{t}\ +c_{3}\sum_{n=0}^{\infty}b_{n}\,Q_{n}^{(5)}\left(\tilde{x}\right),&\end{aligned} \tag{73}$$

with $\tilde{x}=x/a$ and $\tilde{d}=d/a$. The function $Q_{n}^{(5)}\left(\tilde{x}\right)$ is defined as

$$Q_{n}^{(5)}\left(\tilde{x}\right)\equiv\int_{-1}^{1}U_{n}\left(\tilde{t}\right)\left(1-\tilde{t}^{2}\right)^{3/2}R_{5}\left(a\tilde{x}-a\tilde{t}\right)d\tilde{t}\ . \tag{74}$$

The hyper-singular and weakly singular integrals in Eq. (73) are evaluated in closed form in Appendix B (Eq. (B4), (B3) and (B6)) whereas the regular integral in Eq. (74) is calculated based on the standard Gauss-Chebyshev quadrature. In light of the above, the singular integral equation admits the following discretized form

$$
\begin{aligned}
-t_{yz}^{\left(b_{zy}\right)}\left(a\tilde{x}-a\tilde{d},\,0\right) &= -\frac{3c_1\ell^2}{a^2}\Big\{b_0\pi + b_1 4\pi U_1\left(\tilde{x}\right) + b_2\left[3\pi U_0\left(\tilde{x}\right) + 10\pi U_2\left(\tilde{x}\right)\right] \\
&+ b_3 4\pi\left[2U_1\left(\tilde{x}\right) + 5\pi U_3\left(\tilde{x}\right)\right] + \sum_{n=4}^{\infty} b_n \frac{\pi}{96\left(1-\tilde{x}^2\right)^2}\Big[\left(n^3+6n^2+11n+6\right)U_{n+4}\left(\tilde{x}\right) \\
&- \left(4n^3+18n^2+44n+30\right)U_{n+2}\left(\tilde{x}\right) + \left(6n^3+18n^2+54n+42\right)U_n\left(\tilde{x}\right) \\
&- \left(4n^3+6n^2+20n+18\right)U_{n-2}\left(\tilde{x}\right) + \left(n^3-n\right)U_{n-4}\left(\tilde{x}\right)\Big]\Big\} \\
&+ c_2\left\{-b_0\frac{3\pi}{4}\left[U_0\left(\tilde{x}\right) - U_2\left(\tilde{x}\right)\right] - b_1\pi\left[U_1\left(\tilde{x}\right) - U_3\left(\tilde{x}\right)\right]\right. \\
&\left. + \sum_{n=2}^{\infty} b_n \frac{\pi}{4}\left[\left(n-1\right)U_{n-2}\left(\tilde{x}\right) - 2\left(n+1\right)U_n\left(\tilde{x}\right) + \left(n+3\right)U_{n+2}\left(\tilde{x}\right)\right]\right\} \\
&- \frac{\mu a^2}{32\ell^2}\left\{b_0\frac{\pi}{4}\left[T_2\left(\tilde{x}\right) - \frac{1}{8}T_4\left(\tilde{x}\right) - \frac{3}{2}\ln 2\right] - b_1\frac{\pi}{4}\left[T_1\left(\tilde{x}\right) - \frac{1}{2}T_3\left(\tilde{x}\right) + \frac{1}{10}T_5\left(\tilde{x}\right)\right]\right. \\
&- b_2\frac{\pi}{16}\left[3T_2\left(\tilde{x}\right) - \frac{3}{2}T_4\left(\tilde{x}\right) + \frac{1}{3}T_6\left(\tilde{x}\right) - 2\ln 2\right] \\
&\left. + \sum_{n=3}^{\infty} b_n \frac{\pi}{8}\left[\frac{T_{n-2}\left(\tilde{x}\right)}{n-2} - \frac{3T_n\left(\tilde{x}\right)}{n} + \frac{3T_{n+2}\left(\tilde{x}\right)}{n+2} - \frac{T_{n+4}\left(\tilde{x}\right)}{n+4}\right]\right\} + c_3\sum_{n=1}^{\infty} b_n\, Q_n\left(\tilde{x}\right), \quad \left|\tilde{x}\right| < 1.
\end{aligned}
\tag{75}
$$

Eq. (75) is then solved numerically using the same collocation method as in previous sections. Finally, after obtaining a solution for the parameters b_n, we calculate the screw dislocation dipole density using Eq. (72).

6. Energy release rate and Peach-Koehler force evaluation

In this section, we derive the expressions for the energy release rate (J-integral) in both crack-tips and the Peach-Koehler force exerted on the climb dislocation dipole and study their dependence on the material and geometrical parameters of the problem. Atkinson and Leppington (1974) were the first to derive the energy release rate in the context of couple-stress elasticity and prove its path independence (Atkinson and Leppington, 1977).

In order to evaluate the J-integral, we use a rectangular shaped integration path that surrounds the (left or right) crack-tip and has vanishing height along the y-direction, while $\varepsilon \to +0$ (Fig. 4). The benefit of this approach is that only the asymptotic near tip stress and displacement fields suffice for the evaluation of the J-integral. This computationally convenient concept was introduced by Freund (1972) to calculate the energy flux during dynamic crack

propagation and has been later adopted to compute energy quantities in the vicinity of crack-tips (see e.g. Baxevanakis et al., 2017a; Burridge, 1976; Georgiadis, 2003; Gourgiotis and Piccolroaz, 2014).

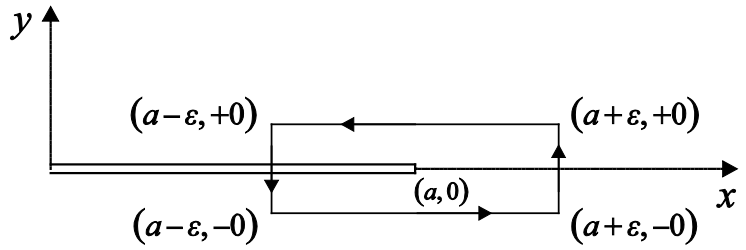

Fig. 4: Rectangular shaped contour for the calculation of J-integral around the right crack-tip.

6.1 Interaction of a finite-length crack with a climb dislocation dipole

Taking into account that in the opening mode problem the shear stress σ_{yx} vanishes for $y = 0$ and the crack faces are defined by $\mathbf{n} = \left(0, \pm 1\right)$, the J-integral admits the following form (see also Baxevanakis et al. (2017a))

$$J = -2 \lim_{\varepsilon \to +0} \left\{ \int_{\pm a - \varepsilon}^{\pm a + \varepsilon} \left[\sigma_{yy}\left(x, 0^+\right) \frac{\partial u_y\left(x, 0^+\right)}{\partial x} + m_{yz}\left(x, 0^+\right) \frac{\partial \omega\left(x, 0^+\right)}{\partial x} \right] dx \right\} . \tag{76}$$

The dominant near crack-tip behavior for the normal stress σ_{yy} and the couple-stress m_{yz} is attributed to the hyper-singular integrals of quadratic singularity in Eqs. (54) and (55), respectively. The asymptotic behavior of these quantities near the right $\left(x \to a^+\right)$ and left $\left(x \to a^-\right)$ crack-tips is given as (see Eq. (B8) in Appendix B)

$$\begin{cases} \sigma_{yy}\left(x \to a^+, 0^+\right) = \dfrac{\mu\left(3 - 2\nu\right)}{2\sqrt{2}\left(1 - \nu\right)} \displaystyle\sum_{n=1}^{N} \left(n + 1\right) b_n \left(\tilde{x} - 1\right)^{-1/2} \\ \sigma_{yy}\left(x \to -a^-,\, 0^+\right) = -\dfrac{\mu\left(3 - 2\nu\right)}{2\sqrt{2}\left(1 - \nu\right)} \displaystyle\sum_{n=1}^{N} \left(-1\right)^n \left(n + 1\right) b_n \left|\tilde{x} + 1\right|^{-1/2} \end{cases}, \quad \left|\tilde{x}\right| > 1 , \tag{77}$$

$$\begin{cases} m_{yz}\big(x\to a^{+},0^{+}\big)=-\dfrac{\sqrt{2}\mu\ell^{2}}{a}\displaystyle\sum_{n=1}^{N}\big(n+1\big)c_{n}\big(\tilde{x}-1\big)^{-1/2} \\ m_{yz}\big(x\to -a^{-},0^{+}\big)=\dfrac{\sqrt{2}\mu\ell^{2}}{a}\displaystyle\sum_{n=1}^{N}\big(-1\big)^{n}\big(n+1\big)c_{n}\big|\tilde{x}+1\big|^{-1/2} \end{cases}, \quad \big|\tilde{x}\big|>1\,. \tag{78}$$

Accordingly, based on the definitions of the defect densities $B_{I}\big(t\big)$ and $W\big(t\big)$ (Eq. (56)), we derive the following relations for the gradients of the displacement and rotation

$$\begin{cases} \dfrac{\partial u_{y}\big(x\to a^{-},0^{+}\big)}{\partial x}=-\dfrac{1}{2\sqrt{2}}\displaystyle\sum_{n=1}^{N}\big(n+1\big)b_{n}\big(1-\tilde{x}\big)^{-1/2} \\ \dfrac{\partial u_{y}\big(x\to -a^{+},\,0^{+}\big)}{\partial x}=-\dfrac{1}{2\sqrt{2}}\displaystyle\sum_{n=1}^{N}\big(-1\big)^{n}\big(n+1\big)b_{n}\big(1+\tilde{x}\big)^{-1/2} \end{cases}, \quad \big|\tilde{x}\big|<1\,, \tag{79}$$

$$\begin{cases} \dfrac{\partial \omega\big(x\to a^{-},0^{+}\big)}{\partial x}=\dfrac{1}{2\sqrt{2}\,a}\displaystyle\sum_{n=1}^{N}\big(n+1\big)c_{n}\big(1-\tilde{x}\big)^{-1/2} \\ \dfrac{\partial \omega\big(x\to -a^{+},0^{+}\big)}{\partial x}=\dfrac{1}{2\sqrt{2}\,a}\displaystyle\sum_{n=1}^{N}\big(-1\big)^{n}\big(n+1\big)c_{n}\big(1+\tilde{x}\big)^{-1/2} \end{cases}, \quad \big|\tilde{x}\big|<1\,. \tag{80}$$

Based on Eqs. (77)-(80), the J-integral at the right crack-tip is written under the form

$$\begin{aligned} J_{r} &= -2a\lim_{\varepsilon\to 0}\left\{-\frac{\mu}{2}\left[\Lambda_{1}^{(r)}+\left(\frac{\ell}{a}\right)^{2}\Lambda_{2}^{(r)}\right]\int_{-\varepsilon/a}^{\varepsilon/a}\big(x_{+}\big)^{-1/2}\cdot\big(x_{-}\big)^{-1/2}\,d\overline{x}\right\} \\ &= \frac{\mu\pi a}{2}\left[\Lambda_{1}^{(r)}+\left(\frac{\ell}{a}\right)^{2}\Lambda_{2}^{(r)}\right], \end{aligned} \tag{81}$$

where

$$\Lambda_{1}^{(r)}=\frac{\big(3-2\nu\big)}{4\big(1-\nu\big)}\left(\sum_{n=0}^{N}\big(n+1\big)b_{n}\right)^{2}, \qquad \Lambda_{2}^{(r)}=\left(\sum_{n=0}^{N}\big(n+1\big)c_{n}\right)^{2}, \tag{82}$$

and $\overline{x}=\tilde{x}-1$. Note that for any real number λ, excluding the values $\lambda=-1,-2,-3,\ldots$, the distributions of the bisection type x_{+}^{λ} and x_{-}^{λ} in Eq. (81) are defined as (Gel'fand and Shilov, 1964)

$$x_+^{\lambda}=\begin{cases}\left|\overline{x}\right|^{\lambda}\,, & \overline{x}>0\\ \\ 0\,, & \overline{x}<0\end{cases}\qquad\text{and}\qquad x_-^{\lambda}=\begin{cases}0\,, & \overline{x}>0\\ \\ \left|\overline{x}\right|^{\lambda}\,, & \overline{x}<0\end{cases}\,. \tag{83}$$

The integral in Eq. (81) is evaluated using Fisher's theorem for products of distributions of the bisection type (Fisher, 1971). Specifically, we use the relation $\left(x_+\right)^{-1-\lambda}\left(x_-\right)^{\lambda}=-\pi\delta\left(x\right)\left[2\sin\left(\pi\lambda\right)\right]^{-1}$, where $\lambda\neq -1,-2,-3,...$ and $\delta\left(x\right)$ is the Dirac delta distribution, together with the fundamental property of the Dirac delta distribution, i.e., $\int_{-\varepsilon}^{\varepsilon}\delta\left(x\right)dx=1\,.$

A similar procedure is followed to derive the J-integral value at the left crack-tip, which is given by the expression

$$\begin{aligned}J_{\ell}&=-2a\lim_{\varepsilon\to 0}\left\{\frac{\mu}{2}\left[\Lambda_1^{(\ell)}+\left(\frac{\ell}{a}\right)^2\Lambda_2^{(\ell)}\right]\int_{-\varepsilon/a}^{\varepsilon/a}\left(x_+\right)^{-1/2}\cdot\left(x_-\right)^{-1/2}d\overline{x}\right\}\\&=-\frac{\mu\pi a}{2}\left[\Lambda_1^{(\ell)}+\left(\frac{\ell}{a}\right)^2\Lambda_2^{(\ell)}\right],\end{aligned} \tag{84}$$

where

$$\Lambda_1^{(\ell)}=\frac{\left(3-2\nu\right)}{4\left(1-\nu\right)}\left(\sum_{n=0}^{N}\left(-1\right)^n\left(n+1\right)b_n\right)^2\,,\qquad \Lambda_2^{(\ell)}=\left(\sum_{n=0}^{N}\left(-1\right)^n\left(n+1\right)c_n\right)^2\,. \tag{85}$$

In the framework of classical elasticity, the J-integral value may be derived in closed form using a similar integration path to the one employed earlier and the elastic fields of the problem. Based on this procedure, we derive the expressions for the J-integral at both crack-tips as

$$J_r^{clas.}=\frac{\mu b_y^2 w_d^2}{8\pi a\left(1-\nu\right)\left(d^2-a\right)\left(d-a\right)^2}\,,\quad J_{\ell}^{clas.}=-\frac{\mu b_y^2 w_d^2}{8\pi a\left(1-\nu\right)\left(d^2-a\right)\left(d+a\right)^2}\,. \tag{86}$$

To the best of our knowledge, these expressions were not available in the literature and are provided herein for the first time.

Moreover, we evaluate the configurational Peach-Koehler force that is exerted on the climb dislocation dipole. To this aim, considering a contour that surrounds both the crack and the infinitesimal climb dislocation dipole (Fig. 5) and using the equilibrium relation between Peach-Koehler force and J-integral around a discrete dislocation (Eshelby, 1951), we may write the expression

$$F_x^{dd} = F_x^{sd1} - F_x^{sd2} = -\big(J_r + J_\ell\big) \ , \tag{87}$$

where F_x^{dd} is the Peach-Koehler force exerted on the dislocation dipole along the x-direction, F_x^{sd1} and F_x^{sd2} (or equivalently J_{d1} and J_{d2}) are the Peach-Koehler forces exerted on the closer and farther to the crack constituent dislocations of the dislocation dipole, while J_r and J_ℓ are the J-integral values at the right and left crack-tip. In Section 7.1, the Peach-Koehler force exerted on the dipole is calculated based on its definition and verified using Eq. (87). Finally, the corresponding Peach-Koehler force for this problem in classical elasticity is derived in the form

$$F_x^{dd,clas.} = -\frac{\mu b_y^2 w_d^2 d}{2\pi\big(1-\nu\big)\big(d^2-a\big)\big(d^2-a^2\big)^2} \ . \tag{88}$$

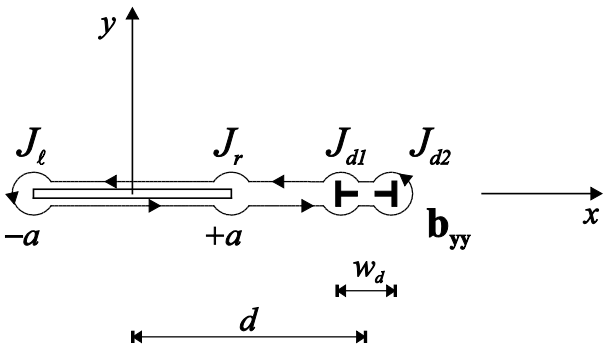

Fig. 5: Contour for the calculation of the Peach-Koehler force around the climb dislocation dipole.

6.2 Interaction of a finite-length crack with a glide dislocation dipole

In the plane shear case, considering that the normal stress σ_{yy} and the couple-stress m_{yz} vanish for $y=0$, the J-integral is given by the following form (see also Baxevanakis et al. (2017b))

$$J=-2\lim_{\varepsilon\to+0}\left\{\int_{\pm a-\varepsilon}^{\pm a+\varepsilon}\sigma_{yx}\left(x,\,0^{+}\right)\frac{\partial u_{x}\left(x,\,0^{+}\right)}{\partial x}dx\right\}\,. \tag{89}$$

The dominant near crack-tip behavior for the shear stress σ_{yx} is attributed to the hyper-singular integral of quadratic singularity in Eq. (64). The asymptotic behavior of this stress near the right $\left(x\to a^{+}\right)$ and left $\left(x\to a^{-}\right)$ crack-tips is given as (see Eq. (B8) in Appendix B)

$$\begin{cases}\sigma_{yx}\left(x\to a^{+},0^{+}\right)=\dfrac{\mu\left(3-2\nu\right)}{2\sqrt{2}\left(1-\nu\right)}\displaystyle\sum_{n=1}^{N}\left(n+1\right)b_{n}\left(\tilde{x}-1\right)^{-1/2}\\ \sigma_{yx}\left(x\to -a^{-},\,0^{+}\right)=-\dfrac{\mu\left(3-2\nu\right)}{2\sqrt{2}\left(1-\nu\right)}\displaystyle\sum_{n=1}^{N}\left(-1\right)^{n}\left(n+1\right)b_{n}\left|\tilde{x}+1\right|^{-1/2}\end{cases},\qquad \left|\tilde{x}\right|>1\,. \tag{90}$$

Accordingly, based on the definition of the glide dislocation dipole density $B_{II}\left(t\right)$, the following asymptotic relations are obtained for the gradient of the tangential displacement

$$\begin{cases}\dfrac{\partial u_{x}\left(x\to a^{-},0^{+}\right)}{\partial x}=-\dfrac{1}{2\sqrt{2}}\displaystyle\sum_{n=1}^{N}\left(n+1\right)b_{n}\left(1-\tilde{x}\right)^{-1/2}\\ \dfrac{\partial u_{x}\left(x\to -a^{+},\,0^{+}\right)}{\partial x}=-\dfrac{1}{2\sqrt{2}}\displaystyle\sum_{n=1}^{N}\left(-1\right)^{n}\left(n+1\right)b_{n}\left(1+\tilde{x}\right)^{-1/2}\end{cases},\qquad \left|\tilde{x}\right|<1\,. \tag{91}$$

Using the same rectangular shaped contour as in the previous section and employing the asymptotic results of Eqs. (90) and (91) in conjunction with Fisher's theorem for products of singular distributions, we eventually derive the following forms for the J-integral in the right and left crack-tips

$$
\begin{aligned}
J_{r} &= -2a \lim_{\varepsilon \to 0} \left\{ -\frac{\mu}{2} \Lambda_{3}^{(r)} \int_{-\varepsilon/a}^{\varepsilon/a} \left(x_{+} \right)^{-1/2} \cdot \left(x_{-} \right)^{-1/2} d\overline{x} \right\} = \frac{\mu \pi a}{2} \Lambda_{3}^{(r)}, \\
J_{\ell} &= -2a \lim_{\varepsilon \to 0} \left\{ \frac{\mu}{2} \Lambda_{3}^{(\ell)} \int_{-\varepsilon/a}^{\varepsilon/a} \left(x_{+} \right)^{-1/2} \cdot \left(x_{-} \right)^{-1/2} d\overline{x} \right\} = -\frac{\mu \pi a}{2} \Lambda_{3}^{(\ell)},
\end{aligned}
\tag{92}
$$

where

$$
\Lambda_{3}^{(r)} = \frac{\left(3 - 2\nu \right)}{4\left(1 - \nu \right)} \left(\sum_{n=0}^{N} \left(n + 1 \right) b_{n} \right)^{2} \quad , \qquad \Lambda_{3}^{(\ell)} = \frac{\left(3 - 2\nu \right)}{4\left(1 - \nu \right)} \left(\sum_{n=0}^{N} \left(-1 \right)^{n} \left(n + 1 \right) b_{n} \right)^{2} \quad . \tag{93}
$$

Finally, the J-integral expressions in classical elasticity are analogous to Eq. (86).

6.3 Interaction of a finite-length crack with a screw dislocation dipole

In the antiplane crack problem, the couple-stress m_{yx} vanishes for $y = 0$ so that the J-integral takes the following form

$$
J = -2 \lim_{\varepsilon \to +0} \left\{ \int_{\pm a - \varepsilon}^{\pm a + \varepsilon} t_{yz} \left(x, \, 0^{+} \right) \frac{\partial w \left(x, \, 0^{+} \right)}{\partial x} dx \right\} \, . \tag{94}
$$

The dominant near crack-tip for the shear stress t_{yz} is attributed to the hyper-singular of the fourth order in Eq. (69). The asymptotic behavior of this stress component near the right $\left(x \to a^{+} \right)$ and left $\left(x \to a^{-} \right)$ crack-tips is given as follows (see Eq. (B10) in Appendix B)

$$
\begin{cases}
t_{yz} \left(x \to a^{+}, \, 0^{+} \right) = -\dfrac{3 c_{1} \ell^{2}}{a^{2}} \dfrac{\pi}{4\sqrt{2}} \displaystyle\sum_{n=1}^{N} \left(n + 1 \right) b_{n} \left(\tilde{x} - 1 \right)^{-3/2} \\
t_{yz} \left(x \to -a^{-}, \, 0^{+} \right) = \dfrac{3 c_{1} \ell^{2}}{a^{2}} \dfrac{\pi}{4\sqrt{2}} \displaystyle\sum_{n=1}^{N} \left(-1 \right)^{n} \left(n + 1 \right) b_{n} \left| \tilde{x} + 1 \right|^{-3/2}
\end{cases}
, \qquad \left| \tilde{x} \right| > 1 \, . \tag{95}
$$

Further, based on the definition of the screw dislocation dipole density $B_{III}\left(t \right)$, the following asymptotic relations are deduced for the gradient of the antiplane displacement

$$\begin{cases} \dfrac{\partial w\big(x \to a^{-},\, 0^{+}\big)}{\partial x} = -\dfrac{3}{\sqrt{2}} \displaystyle\sum_{n=1}^{N} \big(n+1\big) b_n \big(1-\tilde{x}\big)^{1/2} \\ \dfrac{\partial w\big(x \to -a^{+},\, 0^{+}\big)}{\partial x} = -\dfrac{3}{\sqrt{2}} \displaystyle\sum_{n=1}^{N} \big(-1\big)^n \big(n+1\big) b_n \big(1-\tilde{x}\big)^{1/2} \end{cases} , \quad \big|\tilde{x}\big| < 1 \,. \tag{96}$$

Based on the previous results, we derive the expression for the J-integral in both crack-tips as

$$\begin{aligned} J_{r} &= -2a \lim_{\varepsilon \to 0} \left\{ \Lambda_4^{(r)} \int_{-\varepsilon/a}^{\varepsilon/a} \big(x_{+}\big)^{-3/2} \cdot \big(x_{-}\big)^{1/2} \, d\overline{x} \right\} = \pi a \, \Lambda_4^{(r)}, \\ J_{\ell} &= -2a \lim_{\varepsilon \to 0} \left\{ \Lambda_4^{(\ell)} \int_{-\varepsilon/a}^{\varepsilon/a} \big(x_{+}\big)^{1/2} \cdot \big(x_{-}\big)^{-3/2} \, d\overline{x} \right\} = -\pi a \, \Lambda_4^{(\ell)}, \end{aligned} \tag{97}$$

where

$$\Lambda_4^{(r)} = \frac{9\pi c_1 \ell^2}{8a^2} \left(\sum_{n=0}^{N} \big(n+1\big) b_n \right)^2 , \qquad \Lambda_4^{(\ell)} = \frac{9\pi c_1 \ell^2}{8a^2} \left(\sum_{n=0}^{N} \big(-1\big)^n \big(n+1\big) b_n \right)^2 . \tag{98}$$

It is noted that the distributions of the bisection type $x_{+}^{-3/2}$ and $x_{-}^{1/2}$ in Eq. (97) are defined in Eq. (83). In addition, for the evaluation of the integral in Eq. (97), we employ Fisher's theorem so that the product of distributions is computed as $\big(x_{+}\big)^{-3/2} \cdot \big(x_{-}\big)^{1/2} = -2^{-1}\pi\delta\big(x\big)$.

Finally, the J-integral value in classical elasticity may be calculated in closed form utilizing a similar contour as the one used earlier and the expressions of the elastic fields of the problem (Lin et al., 1993). Based on this procedure, we obtain the following forms for the J-integral at the right and left crack-tips

$$J_{r}^{clas.} = \frac{\mu b_z^2 w_d^2}{8\pi a \big(d^2 - a\big)\big(d-a\big)^2} , \qquad J_{\ell}^{clas.} = -\frac{\mu b_z^2 w_d^2}{8\pi a \big(d^2 - a\big)\big(d+a\big)^2} . \tag{99}$$

7. Results and discussion

In this section, we present and discuss characteristic results obtained for the three interaction problems. It is noted that an exhaustive parametric study was not conducted in this work, however, comments for limit cases are provided where appropriate. The objective of this section

is to highlight the deviations from the classical elasticity theory when couple-stresses are considered.

7.1 Interaction of a finite-length crack with a climb dislocation dipole

In Fig. 6a, the effect of the ratio a/ℓ on the normal crack face displacement (Eq. (56)) is explored for a climb dislocation dipole lying at a distance $d/a = 2.5$ in a couple-stress material with Poisson's ratio $\nu = 0.3$. We observe that the displacements become smaller in magnitude as the characteristic length becomes comparable to the crack length, i.e. the material exhibits a stiffer behavior. Due to the nature of the loading, the obtained displacement profile is always asymmetric, which becomes more evident when the defect is placed close to the crack-tip. It is also noted the classical elasticity solution (dashed line) is an upper bound for couple-stress elasticity.

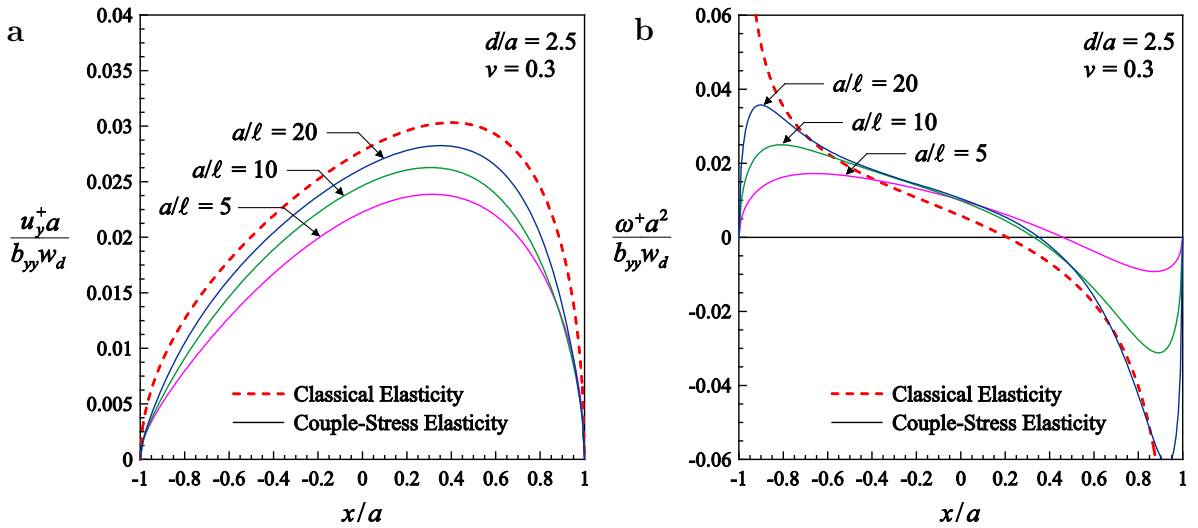

Fig. 6: a) Normalized upper-half crack displacement and b) rotation profiles for various ratios a/ℓ due to the interaction with a climb dislocation dipole lying at $d/a = 2.5$ in a material with $\nu = 0.3$.

Accordingly, using Eq. (56), we evaluate the upper-half crack rotation for the same configuration. In Fig. 6b the variation of the rotation with respect to the ratio a/ℓ is presented. It should be emphasized that the results in couple-stress theory are *bounded* and tend to zero in both crack-tips. On the contrary, the classical elasticity solution (dashed line) exhibits a square-

root singularity at the crack-tips. We also note that as $\ell \to 0$, the rotation in couple-stress elasticity becomes pointwise convergent to the classical elasticity unbounded solution. Both the displacement and the rotation of the crack faces are significantly affected by the distance of the dipole from the crack-tip. In general, the produced fields are smaller in magnitude compared to the interaction of a finite-length crack with a discrete climb dislocation (Baxevanakis et al., 2017a). This response is expected since the stress field of a dislocation dipole diminishes more rapidly over the distance than that of a discrete dislocation.

Moreover, we study the behavior of the normal stress σ_{yy} and the couple-stressς m_{yz} ahead of the crack-tip. From the superposition of the two auxiliary problems, we derive the expressions (see Eqs. (54) and (55))

$$\begin{aligned}\sigma_{yy}\left(\left|x\right|>a,\,0\right)=\sigma_{yy}^{\left(b_{yy}\right)}\left(x-d,\,0\right)+\frac{\mu\left(3-2\nu\right)}{2\pi\left(1-\nu\right)}\int_{-a}^{a}\frac{B_I\left(t\right)}{\left(x-t\right)^2}dt\\ -\frac{\mu}{\pi a}\int_{-a}^{a}\frac{W\left(t\right)}{x-t}dt-\frac{\mu}{4\pi\ell^2}\int_{-a}^{a}B_I\left(t\right)\ln\frac{\left|x-t\right|}{\ell}dt\\ +\frac{\mu}{\pi}\int_{-a}^{a}B_I\left(t\right)R_1\left(x-t\right)dt\ +\frac{\mu}{\pi a}\int_{-a}^{a}W\left(t\right)R_2\left(x-t\right)dt\ ,\end{aligned}\tag{100}$$

$$\begin{aligned}m_{yz}\left(\left|x\right|>a,\,0\right)=m_{yz}^{\left(b_{yy}\right)}\left(x-d,\,0\right)+-\frac{2\mu\ell^2}{\pi a}\int_{-a}^{a}\frac{W\left(t\right)}{\left(x-t\right)^2}dt-\frac{\mu}{\pi}\int_{-a}^{a}\frac{B_I\left(t\right)}{x-t}dt\\ -\frac{\mu}{\pi a}\int_{-a}^{a}W\left(t\right)\ln\frac{\left|x-t\right|}{\ell}dt+\frac{\mu}{\pi}\int_{-a}^{a}B_I\left(t\right)R_2\left(x-t\right)dt\ +\frac{\mu}{\pi a}\int_{-a}^{a}W\left(t\right)R_3\left(x-t\right)dt\ .\end{aligned}\tag{101}$$

For $\left|x\right|>a$, the integrals in Eqs. (100) and (101) are not singular and are evaluated in closed form in Appendix B (Eqs. (B8), (B7) and (B11)). Also, in view of Eqs. (77) and (78) it is deduced that both the normal stress σ_{yy} and the couple-stress m_{yz} exhibit a square-root singularity ahead of the crack-tips.

The distribution of the normal stress σ_{yy} (Eq. (100)) due to the interaction with a climb dislocation dipole placed at a distance $d/a=2.5$ is plotted in Fig 7a, in a medium with

$a/\ell = 10$ and Poisson's ratio $\nu = 0.3$. In the x-axis, the distance is measured from the right crack-tip where a new variable, $\overline{x} = x - a$, is introduced for convenience. Comparing this response with the classical elasticity solution, we observe that the couple-stress effects are visible within a zone of 10ℓ around the defect center and 3ℓ near the crack-tip. Outside this range, the stress distribution approaches the classical elasticity response. The width of these zone varies with the distance between the defect and the crack-tip. In general, the normal stress distribution depends on the ratio a/ℓ and the Poisson's ratio (see Eq. (100)), however, the response is always qualitatively similar to the one reported in this plot. It is also mentioned that the square-root singularity induced by the dislocation dipole is retained in couple-stress theory.

The distribution of the couple-stress m_{yz} is presented in Fig7b. In this example, the couple-stress effects are evident in a zone of length 15ℓ around the dipole center and 2ℓ ahead of the crack-tip. Again, the length of these zones will extend if the dislocation dipole is placed farther from the crack-tip. It is also noted that for $\overline{x}/\ell = 15$ (dipole center), the couple-stress field exhibits a Cauchy type singularity, as described in Eqs. (44)-(46).

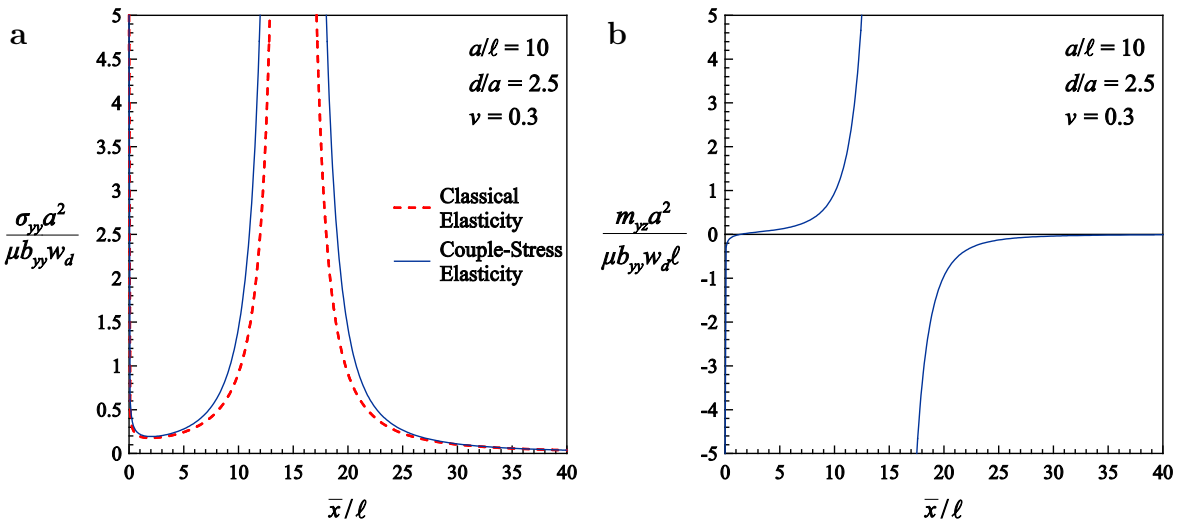

Fig. 7: Variation of (a) the normal stress σ_{yy} and (b) the couple-stress m_{yz} ahead of the right crack-tip due to the interaction with a climb dislocation dipole lying at $d/a = 2.5$ in a medium with $a/\ell = 10$ and Poisson's ratio $\nu = 0.3$.

Moreover, we study the variation of the stress intensity factor (SIF) in couple-stress theory at both crack-tips. The SIF is defined at the right crack-tip as

$K_I = \lim_{x \to a^+} \left[2\pi \left(x - a \right) \right]^{1/2} \sigma_{yy} \left(x, 0 \right)$, where the asymptotic behavior of the normal stress $\sigma_{yy} \left(x, 0 \right)$ is given in Eq. $(77)_1$. The definition at the left crack-tip is similar. At this point, we compare the convergence of the displacement-based formulation of the opening mode crack problem to that of the slope formulation (Baxevanakis et al., 2017a). To achieve this, we revisit the interaction problem of a finite-length crack with a discrete climb dislocation and update the left hand side of the system of integral equations (54) and (55) to accommodate that loading (see Appendix A in Baxevanakis et al. (2017a)). The investigation of solution convergence with respect to the ratio ℓ / a based on the current approach is summarized in Table 1. Comparing these results to those obtained by the slope based method (Table 1 in Baxevanakis et al. (2017a)), we deduce that less terms are required in the current formulation for a given level of accuracy. Also, the relative error in the results derived by coarse grids (i.e. $N = 10$) is smaller than in the discrete dislocation approach.

Table 1: Stress intensity factors ratio in the right crack-tip $K_{I,r} / K_{I,r}^{clas.}$ due to the interaction with a discrete climb dislocation (Baxevanakis et al., 2017a) lying at a distance $d / a = 2.0$ in a material with Poisson's ratio $\nu = 0$.

N	$\ell / a = 1.0$	$\ell / a = 0.8$	$\ell / a = 0.5$	$\ell / a = 0.2$	$\ell / a = 0.1$	$\ell / a = 0.05$	$\ell / a = 0.01$	$\ell / a = 0.005$
10	2.61055	2.47282	2.11816	1.52565	1.35923	1.31378	1.29180	1.35035
20	2.61055	2.47282	2.11816	1.52565	1.35930	1.31382	1.29898	1.28930
30					1.35930	1.31382	1.29933	1.29880
40							1.29945	1.29894
50							1.29945	1.29924
60								1.29924

Returning to the interaction with a climb dislocation dipole, in Fig. 8 the variation of the ratio $K_I / K_I^{clas.}$ in both crack-tips with respect to the ratio ℓ / a and the Poisson's ratio ν is plotted, for a defect placed at a distance $d / a = 2.5$. We notice that the response is highly different in the two crack-tips due to the asymmetric nature of the applied loading. In all cases, the stress intensity factor in couple-stress theory is significantly higher than the classical elasticity solution (stress aggravation effect). The right crack-tip curves (continuous lines) monotonically increase in the range $0 \leq \ell / a \leq 1$ and then decrease and approach asymptotically

the value $\left(3-2\nu\right)$ as $\ell/a \to \infty$. On the contrary, in the left crack-tip response (dashed lines) there is an initial decreasing branch and then a monotonically increasing behavior until the asymptotic value $\left(3-2\nu\right)$ as $\ell/a \to \infty$. Further, for $\ell/a = 0$, the SIFs ratio exhibits a finite jump discontinuity (i.e. $K_I/K_I^{clas.} \neq 1$), which is attributed to the boundary layer effects that arise in couple-stress elasticity in singular stress-concentration problems (Sternberg and Muki, 1967). It is also noted that the general trend of the SIFs ratio response is comparable with the single climb dislocation interaction problem (Baxevanakis et al., 2017a).

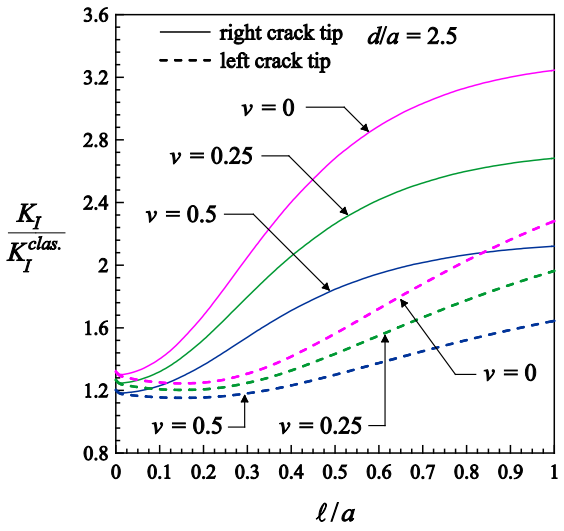

Fig. 8: Variation of the ratio of stress intensity factors in couple-stress theory and in classical elasticity with ℓ/a for a climb dislocation dipole lying at $d/a = 2.5$.

Next, we evaluate numerically the energy release rate, based on Eqs. (81) and (84). In Fig. 9 the dependence of the ratio $J/J^{clas.}$ on the microstructural ratio ℓ/a and the Poisson's ratio ν is depicted, for a climb dislocation dipole lying at a distance $d/a = 2.5$. We note that as the ratio $\ell/a \to 0$, the J-integral in couple-stress theory tends to the corresponding results of classical elasticity. The response shows a similar non-monotonic trend in both crack-tips: as ℓ/a increases, the ratio initially decreases $\left(J < J^{clas.}\right)$ until a minimum value is reached for $0.1 \leq \ell/a \leq 0.15$ (this range varies depending on the Poisson's ratio and the defect distance d/a) and afterwards a monotonically increasing behavior is observed $\left(J > J^{clas.}\right)$. Eventually,

the ratio $J/J^{clas.}$ tends asymptotically to the value $(3-2\nu)$ as $\ell/a \to \infty$. Hence, for small values of ℓ/a, the crack driving force is lower than the corresponding classical elasticity solution revealing a *strengthening* effect while for higher values of the microstructural ratio ℓ/a a *weakening* effect is noticed since $J/J^{clas.} > 1$. A similar 'alternating' behavior was presented in the interaction with discrete plane defects (Baxevanakis et al., 2017a, b).

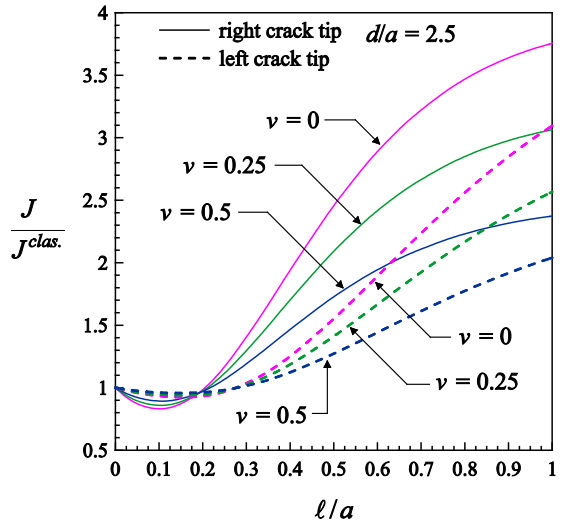

Fig. 9: Variation of the ratio of J-integrals in couple-stress theory and in classical elasticity with ℓ/a for a climb dislocation dipole lying at $d/a = 2.5$.

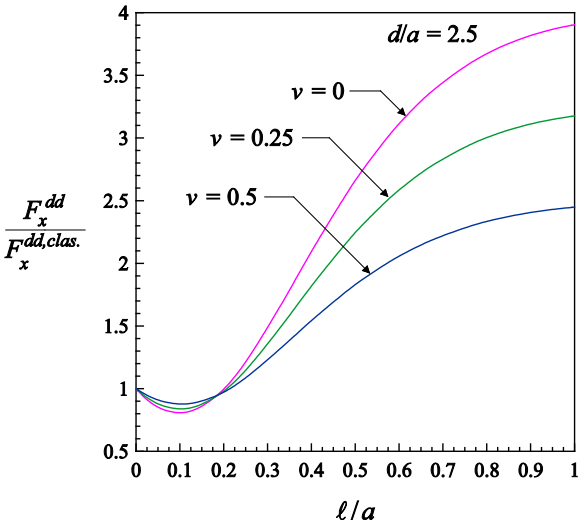

Fig. 10: Variation of the ratio $F_x^{dd}/F_x^{dd,clas.}$ with respect to ℓ/a for a climb dislocation dipole lying at $d/a = 2.5$.

Accordingly, considering the J-integral response, we expect the configurational force exerted on the climb dislocation dipole to exhibit an analogous behavior. In Fig. 10, the variation of the ratio $F_x^{dd}\big/F_x^{dd,clas.}$ is given with respect to the ratio $\ell\big/a$ and the Poisson's ratio ν, for a climb dipole at a distance $d\big/a=2.5$. In accordance to the previous results, the Peach-Kohler force tends to its classical elasticity value for $\ell\big/a\to 0$. Then, as $\ell\big/a$ increases, the ratio $F_x^{dd}\big/F_x^{dd,clas.}$ decreases until a finite minimum value for $\ell\big/a\approx 0.1$ and then increases monotonically. For $\ell\big/a>1$, the ratio decreases until the asymptotic value $\left(3-2\nu\right)$ as $\ell\big/a\to\infty$. Overall, the dislocation dipole driving force is increased in couple-stress elasticity for a large range of values of the ratio $\ell\big/a$.

7.2 Interaction of a finite-length crack with a glide dislocation dipole

We proceed with the presentation of characteristic results for the interaction of a finite-length crack with a glide dislocation dipole. In Fig. 11 the dependence of the tangential crack face displacement on the ratio $a\big/\ell$ is displayed for a glide dislocation dipole placed at a distance $d\big/a=2.5$ in a couple-stress material with Poisson's ratio $\nu=0.3$. In this interaction problem, the displacement profile for a given value of $a\big/\ell$ is reduced more with respect to its classical elasticity counterpart compared to interaction problems studied earlier (see Fig. 6a and Baxevanakis et al. (2017a, 2017b)). For instance, the maximum displacement for $a\big/\ell=20$ is reduced by 6% compared to the corresponding maximum in classical elasticity while for $a\big/\ell=10$ and $a\big/\ell=5$ the maximum values are reduced by 15% and 34% respectively. In the interaction with a discrete glide dislocation (Baxevanakis et al., 2017b), the corresponding reduction percentages are 5%, 10% and 24% for the same three cases of $a\big/\ell$ considered here.

Next, we examine the behavior of the shear stress σ_{yx} ahead of the crack-tip. Superposition of the two auxiliary problems (see Eq. (64)) yields the expression

$$\sigma_{yx}\left(|x|>a,\,0\right)=\sigma_{yx}^{\left(b_{xy}\right)}\left(x-d,\,0\right)+\frac{\mu\left(3-2\nu\right)}{2\pi\left(1-\nu\right)}\int_{-a}^{a}\frac{B_{II}\left(t\right)}{\left(x-t\right)^{2}}dt$$
$$-\frac{3\mu}{4\pi\ell^{2}}\int_{-a}^{a}B_{II}\left(t\right)\ln\frac{|x-t|}{\ell}dt+\frac{\mu}{\pi}\int_{-a}^{a}B_{II}\left(t\right)R_{4}\left(x-t\right)dt\quad. \tag{102}$$

In light of Eq. (90) it is inferred that the shear stress σ_{yx} exhibits a square-root singularity at both crack-tips as in the classical elasticity case.

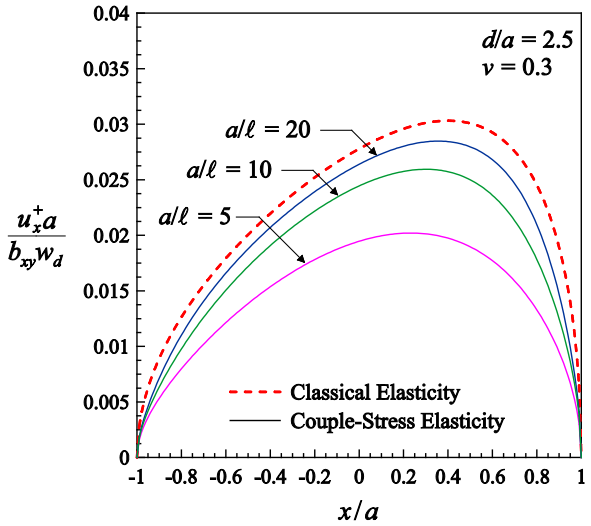

Fig. 11: Normalized upper-half crack tangential displacement profile for various ratios a/ℓ due to the interaction with a glide dislocation dipole lying at $d/a=2.5$ in a material with $\nu=0.3$.

Further, the expression for the couple-stress m_{xz} is derived by integrating Eq. (33) along the crack faces $\left(|x|<a,\;y=0\right)$ and employing results from asymptotic analysis as

$$m_{xz}\left(|x|>a,\,0\right)=m_{xz}^{\left(b_{xy}\right)}\left(x-d,\,0\right)-\frac{\mu}{\pi}\int_{-a}^{a}\frac{B_{II}\left(t\right)}{x-t}dt+\frac{\mu}{\pi}\int_{-a}^{a}B_{II}\left(t\right)R_{6}\left(x-t\right)dt\,, \tag{103}$$

where the regular kernel $R_{6}\left(x-t\right)$ is given as

$$R_6\left(x-t\right)=\frac{4\ell^2}{\left(x-t\right)^3}-\frac{x-t}{\ell^2}\left[K_2\left(\frac{\left|x-t\right|}{\ell}\right)-K_0\left(\frac{\left|x-t\right|}{\ell}\right)\right]+\frac{1}{x-t}\left[1-2K_2\left(\frac{\left|x-t\right|}{\ell}\right)\right].$$

(104)

Using asymptotic analysis as $x\to a^+$, it can be shown that the couple-stress m_{xz} is bounded at the crack-tip.

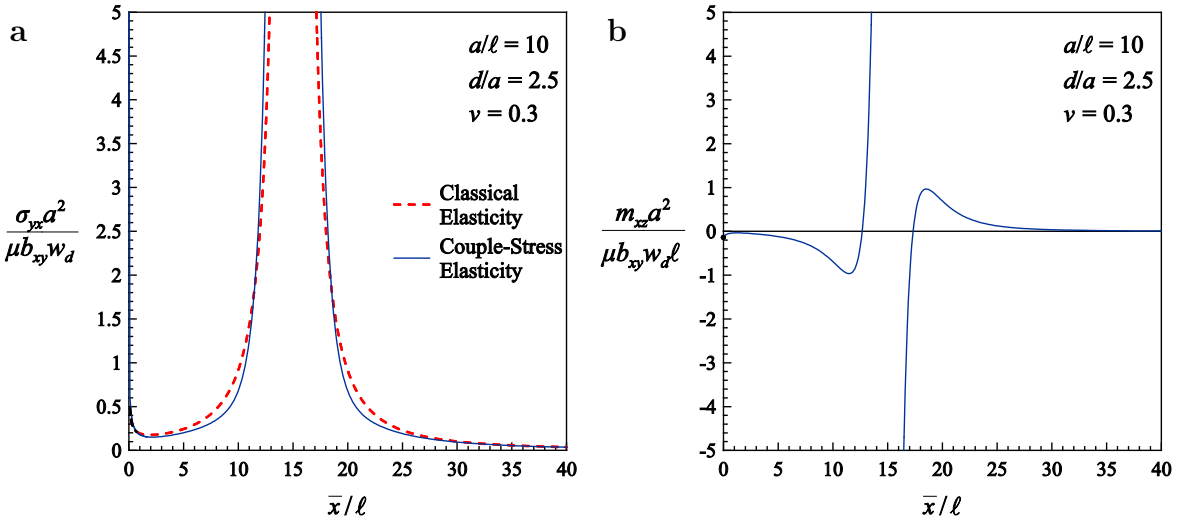

Fig. 12: Variation of a) the shear stress σ_{yx} and b) the couple-stress m_{xz} ahead of the right crack-tip due to the interaction with a glide dislocation dipole lying at $d/a = 2.5$ in a medium with $a/\ell = 10$ and Poisson's ratio $\nu = 0.3$.

In Fig. 12a we present the distribution of the shear stress σ_{yx} for a glide dislocation dipole lying at a distance $d/a = 2.5$ in a couple-stress material with $a/\ell = 10$ and Poisson's ratio $\nu = 0.3$. In this case, it is noted that the couple-stress effects are significant within a zone of 12ℓ around the defect center whereas near the crack-tip the couple-stress result practically coincides with the classical elasticity solution. For different positions of the dislocation dipole, a deviation from the classical elasticity solution near the crack-tip becomes evident. Additionally, as $x\to d$, the field exhibits a quadratic singularity due to the dislocation dipole, as in classical theory. Further, the distribution of the couple-stress m_{xz} is plotted in Fig 12b. The field has a bounded negative value ahead of the crack-tip as discussed earlier and vanishes rapidly to zero as $x > d$. For certain locations of the defect, positive values of the couple-stress m_{xz} are

reported. Finally, around the dislocation dipole $\left(x \to d\right)$, the field exhibits a Cauchy type singularity, as Eq. (33) suggests.

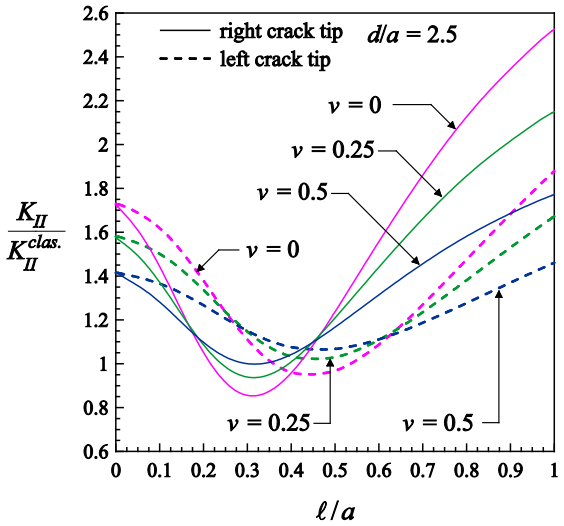

Fig. 13: Variation of the ratio of stress intensity factors in couple-stress theory and in classical elasticity versus ℓ/a for a glide dislocation dipole lying at $d/a = 2.5$.

We now examine the deviation of the stress intensity factor in couple-stress theory from the classical elasticity prediction. For this crack problem, the SIF is defined at the right crack-tip as $K_{II} = \lim_{x \to a^+} \left[2\pi\left(x-a\right)\right]^{1/2} \sigma_{yx}\left(x,\, 0\right)$, where the shear stress $\sigma_{yx}\left(x,\, 0\right)$ is provided in Eq. (102). In Fig. 13, the variation of the ratio $K_{II}/K_{II}^{clas.}$ in both crack-tips with respect to the ratio ℓ/a and the Poisson's ratio ν is shown, for a glide dislocation dipole placed at a distance $d/a = 2.5$. In this example, there is a range where the SIF in couple-stress theory is smaller than the classical theory solution. More specifically, as ℓ/a increases, all curves initially drop until a finite minimum value in the range $0.3 \le \ell/a \le 0.35$ for the right crack-tip and $0.35 \le \ell/a \le 0.45$ for the left crack-tip and then monotonically increase up to the asymptotic value $\left(3-2\nu\right)$ as $\ell/a \to \infty$. The severe boundary layer effects of couple-stress theory are manifested in this graph since for $\ell/a = 0$, the ratio $K_{II}/K_{II}^{clas.} \neq 1$. In general, for different locations of the defect, it may hold that $K_{II} > K_{II}^{clas.}$.

Based on Eq. (92), we evaluate numerically the energy release rate (J-integral). In Fig. 14, the variation of the ratio $J/J^{clas.}$ in both crack-tips is given for various values of the ratio ℓ/a and the Poisson's ratio ν, for a glide dislocation dipole lying at a distance $d/a = 2.5$. It is observed that as $\ell/a \to 0$, the J-integral in couple-stress theory converges to the classical elasticity solution since the ratio $J/J^{clas.}$ tends to unity. The response reported for the J-integral ratio resembles that of the SIFs ratio behavior. Specifically, all curves have an initial decreasing branch until a finite minimum value is reached, which depends on the defect distance d/a and the Poisson's ratio ν and is different for each crack-tip. Then, the ratio $J/J^{clas.}$ shows an increasing behavior and reaches the asymptotic value $(3-2\nu)$ as $\ell/a \to \infty$. Overall, this result is quantitatively similar to the opening mode problem (Fig. 9) and to the interaction problem with a discrete glide dislocation (Baxevanakis et al., 2017b).

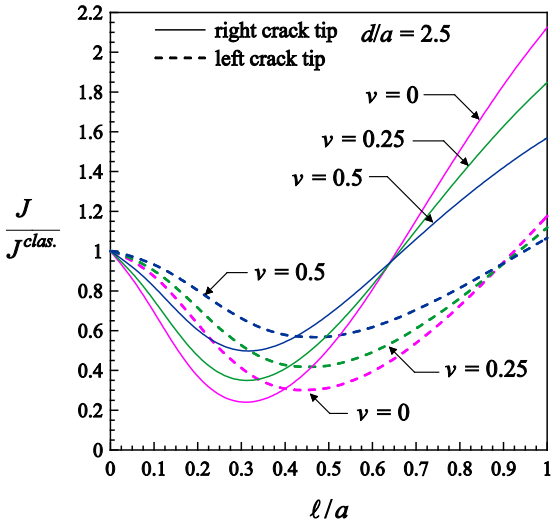

Fig. 14: Variation of the ratio of J-integrals in couple-stress theory and in classical elasticity with respect to the ratio ℓ/a for a glide dislocation dipole lying at $d/a = 2.5$.

7.3 Interaction of a finite-length crack with a screw dislocation dipole

In this paragraph, we present and discuss the results of the antiplane problem. The effect of the ratio a/ℓ on the antiplane displacement w is shown in Fig. 15, for a screw dislocation dipole placed at a distance $d/a = 2.5$ in a couple-stress material with $\beta = 0$. Looking at the

magnification of the profile at the right crack-tip (see figure inset), we deduce that the crack faces close in a smoother way $\left(\overline{x}^{3/2}\right)$ than the classical elasticity prediction, as is supported by Eq. (96). As in the plane problems discussed earlier, we note that the material exhibits a more stiff behavior as the crack length becomes comparable to the characteristic length ℓ. Indeed, the classical elasticity solution is still an upper bound for couple-stress elasticity. Also, the produced displacements are smaller compared to the interaction problem with a discrete screw dislocation (Baxevanakis et al., 2017b), which is expected since dislocation dipoles produce weaker stress fields than discrete dislocations.

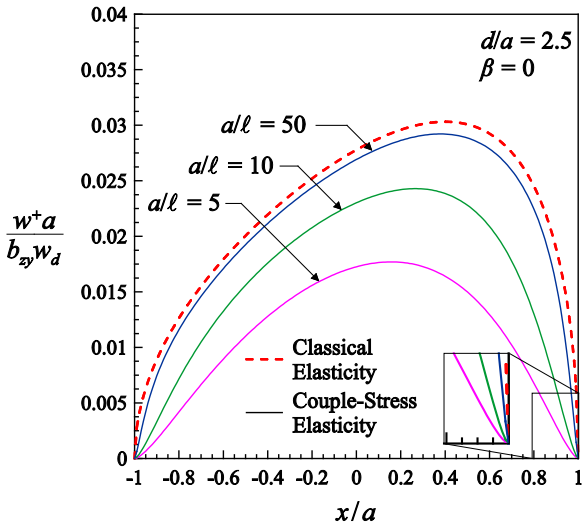

Fig. 15: Normalized upper-half crack antiplane displacement profile for various ratios a/ℓ due to the interaction with a screw dislocation dipole lying at $d/a = 2.5$ in a material with $\beta = 0$.

Next, we evaluate the total shear stress t_{yz} based on Eq. (69) as

$$t_{yz}\left(|x| > a,\, 0\right) = t_{yz}^{(b_{zy})}\left(x-d,\, 0\right) - 3c_1\ell^2\int_{-a}^{a}\frac{B_{III}\left(t\right)}{\left(x-t\right)^4}dt + c_2\int_{-a}^{a}\frac{B_{III}\left(t\right)}{\left(x-t\right)^2}dt$$
$$-\frac{\mu}{32\ell^2}\int_{-a}^{a}B_{III}\left(t\right)\ln\frac{|x-t|}{\ell}dt + c_3\int_{-a}^{a}B_{III}\left(t\right)R_5\left(x-t\right)dt\,, \tag{105}$$

where for $|x| > a$ the integrals are now regular and are evaluated in closed form in Appendix B (Eqs. (B10), (B9), and (B12)). Further, it is reminded that the total stress behaves as $\overline{x}^{-3/2}$ near the crack-tips (Eq. (95)).

In Fig. 16, the distribution of the total shear stress t_{yz} is given due to the interaction with a screw dislocation dipole lying at $d/a = 2.5$, in a medium with $a/\ell = 500$ and three values of the parameter β. The obtained behavior in couple-stress theory differs significantly from the classical elasticity result (dashed line). The total shear stress t_{yz} exhibits a cohesive-traction character along the prospective fracture zone since it has negative values in a small region $\left(\overline{x} < 0.5\ell\right)$ ahead of both crack-tips. Further, for $\overline{x} < 2\ell$, the distribution exhibits a bounded maximum value while for $\overline{x} > 2\ell$ it tends to the classical elasticity solution. It is also worth mentioning that as $\beta \to -1$, the width of the cohesive-traction zone is reduced and the maximum value of the total shear stress increases.

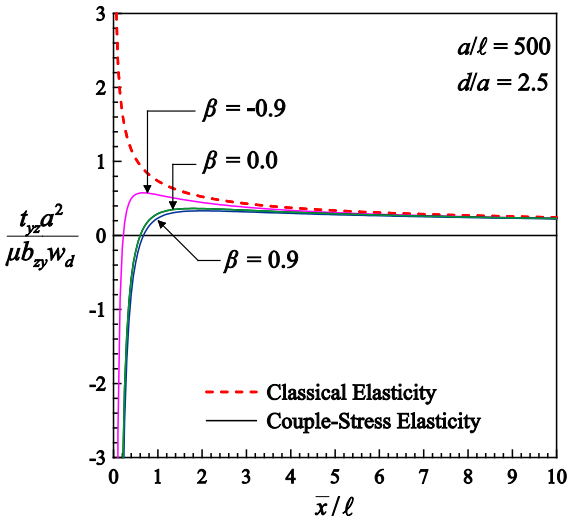

Fig. 16: Variation of the total shear stress t_{yz} ahead of the right crack-tip due to the interaction with a screw dislocation dipole lying at $d/a = 2.5$ in a medium with $a/\ell = 500$ for different values of β.

Then, we evaluate numerically the J-integral at both crack-tips according to Eq. (97). In Fig. 17, the variation of the ratio $J/J^{clas.}$ is plotted with respect to the ratio ℓ/a and the parameter β, for a screw dislocation dipole lying at a distance $d/a = 2.5$. As in the plane strain cases, the ratio $J/J^{clas.}$ tends to unity for $\ell/a \to 0$, that is, the J-integral result in couple-stress

theory reduces to the classical elasticity solution. On the other hand, we observe that in the antiplane case, the ratio $J/J^{clas.} < 1$ as ℓ/a increases. Therefore, the energy release rate decreases when the material microstructure is considered (strengthening effect). This response is independent of the position of the defect. Also, contrary to the plane strain cases, the ratio is always higher at the left crack-tip. Another interesting observation is that the ratio $J/J^{clas.}$ tends to zero for $\beta \geq 0$ and $\ell/a > 0.60$, which is attributed to the nature of the screw dislocation dipole loading.

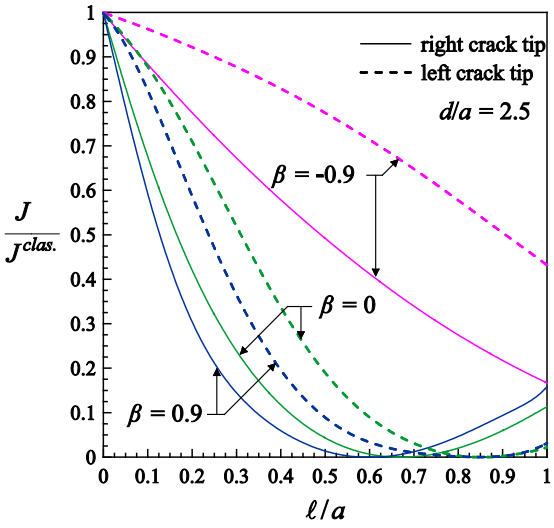

Fig. 17: Variation of the ratio of J-integrals in couple-stress theory and in classical elasticity with ℓ/a for a screw dislocation dipole lying at $d/a = 2.5$.

8. Concluding remarks

In the present study, interaction problems between finite-length cracks and dislocation dipoles were investigated in the context of couple-stress elasticity. The formulation of such problems was achieved by generalizing the distributed dislocation technique and using as nuclei of strain infinitesimal dislocation dipoles. The stress fields of these area defects were derived for the first time in the framework of couple-stress elasticity theory. The displacement-based formulation presented in this work proved to be computationally efficient as less terms are required for a given level of accuracy compared to the classical distributed dislocation technique. In addition, the crack displacement profiles are readily obtained since, in this approach, the distributed defect density coincides with the crack displacement. Using this approach, both the plane strain and

the antiplane crack problems were described by hyper-singular integral equations, which were solved numerically. It is also noted that in order to satisfy the boundary conditions in the opening mode problem, a new rotational defect was introduced, termed as infinitesimal 'constrained' wedge disclination dipole.

Several interesting conclusions can be drawn from this investigation. In all problems, the cracked solid was found to behave in a more rigid way (i.e. the crack face displacements were smaller in magnitude) that the classical elasticity prediction. The generated stress and couple-stress fields are reduced compared to the interaction problems with discrete dislocations, since the loading induced by dislocation dipoles vanishes more rapidly with distance. It was further observed that these fields are altered by couple-stress effects in a small zone ahead of the crack-tip and around the dislocation dipole while they remain unbounded around the defect tips. In the plane shear problem, the stress intensity factor was smaller than its counterpart in classical elasticity for a range of values of the microstructural ratio ℓ/a. In addition, it was shown that the energy release rate is significantly influenced by the defect distance and the magnitude of the characteristic material length with respect to the crack length. Indeed, in the plane strain problems, the energy release rate reveals either strengthening or weakening effects depending on the material parameters and the geometry whereas in the antiplane case, the energy release rate is always decreasing, revealing, thus, a strengthening effect when couple-stresses are considered. The presented crack formulation and obtained results are expected to form the basis for more complex interaction problems of multiple cracks and randomly oriented defects in couple-stress theory.

Appendix A

Following the procedure described in Eqs. (21) and (22), we derive the full-field solution for the stresses and couple-stresses that are generated from the superposition of an infinitesimal climb dislocation dipole (see Eqs. (23)-(28)) and an infinitesimal constrained wedge disclination dipole (Baxevanakis et al., 2017a) as follows

$$\begin{aligned}\sigma_{xx} =& \frac{\mu b_y w_d}{2\pi\left(1-\nu\right)r^2}\cos 4\theta - \frac{6\mu b_y w_d}{\pi r^2}\left[\frac{2\ell^2}{r^2} - K_2\left(\frac{r}{\ell}\right)\right]\cos 4\theta \\ & -\frac{\mu b_y w_d}{4\pi\ell^2}\left\{K_0\left(\frac{r}{\ell}\right) + \left[3K_0\left(\frac{r}{\ell}\right) - 4K_2\left(\frac{r}{\ell}\right)\right]\cos 4\theta\right\} + \frac{2\mu\boldsymbol{\Omega}_z w_d}{\pi r}\cos 3\theta \\ & \times\left[\frac{2\ell^2}{r^2} - K_2\left(\frac{r}{\ell}\right)\right] - \frac{\mu\boldsymbol{\Omega}_z w_d r}{4\pi\ell^2}\left[K_0\left(\frac{r}{\ell}\right) - K_2\left(\frac{r}{\ell}\right)\right]\left(\cos\theta - \cos 3\theta\right),\end{aligned} \tag{A1}$$

$$\begin{aligned}\sigma_{yy} =& \frac{\mu b_y w_d}{2\pi\left(1-\nu\right)r^2}\left(2\cos 2\theta - \cos 4\theta\right) + \frac{6\mu b_y w_d}{\pi r^2}\left[\frac{2\ell^2}{r^2} - K_2\left(\frac{r}{\ell}\right)\right]\cos 4\theta \\ & +\frac{\mu b_y w_d}{4\pi\ell^2}\left\{K_0\left(\frac{r}{\ell}\right) + \left[3K_0\left(\frac{r}{\ell}\right) - 4K_2\left(\frac{r}{\ell}\right)\right]\cos 4\theta\right\} - \frac{2\mu\boldsymbol{\Omega}_z w_d}{\pi r}\cos 3\theta \\ & \times\left[\frac{2\ell^2}{r^2} - K_2\left(\frac{r}{\ell}\right)\right] + \frac{\mu\boldsymbol{\Omega}_z w_d r}{4\pi\ell^2}\left[K_0\left(\frac{r}{\ell}\right) - K_2\left(\frac{r}{\ell}\right)\right]\left(\cos\theta - \cos 3\theta\right),\end{aligned} \tag{A2}$$

$$\begin{aligned}\sigma_{yx} =& -\frac{\mu b_y w_d}{2\pi\left(1-\nu\right)r^2}\left(\sin 2\theta - \sin 4\theta\right) - \frac{6\mu b_y w_d}{\pi r^2}\left[\frac{2\ell^2}{r^2} - K_2\left(\frac{r}{\ell}\right)\right]\sin 4\theta \\ & +\frac{\mu b_y w_d}{4\pi\ell^2}\left\{2K_0\left(\frac{r}{\ell}\right)\sin 2\theta - \left[3K_0\left(\frac{r}{\ell}\right) - 4K_2\left(\frac{r}{\ell}\right)\right]\sin 4\theta\right\} + \frac{2\mu\boldsymbol{\Omega}_z w_d}{\pi r} \\ & \times\left[\frac{2\ell^2}{r^2} - K_2\left(\frac{r}{\ell}\right)\right]\sin 3\theta + \frac{\mu\boldsymbol{\Omega}_z w_d r}{4\pi\ell^2}\left[K_0\left(\frac{r}{\ell}\right) - K_2\left(\frac{r}{\ell}\right)\right]\left(\sin\theta + \sin 3\theta\right),\end{aligned} \tag{A3}$$

$$\begin{aligned}\sigma_{xy} =& -\frac{\mu b_y w_d}{2\pi\left(1-\nu\right)r^2}\left(\sin 2\theta - \sin 4\theta\right) - \frac{6\mu b_y w_d}{\pi r^2}\left[\frac{2\ell^2}{r^2} - K_2\left(\frac{r}{\ell}\right)\right]\sin 4\theta \\ & -\frac{\mu b_y w_d}{4\pi\ell^2}\left\{2K_0\left(\frac{r}{\ell}\right)\sin 2\theta + \left[3K_0\left(\frac{r}{\ell}\right) - 4K_2\left(\frac{r}{\ell}\right)\right]\sin 4\theta\right\} + \frac{2\mu\boldsymbol{\Omega}_z w_d}{\pi r} \\ & \times\left[\frac{2\ell^2}{r^2} - K_2\left(\frac{r}{\ell}\right)\right]\sin 3\theta - \frac{\mu\boldsymbol{\Omega}_z w_d r}{4\pi\ell^2}\left[K_0\left(\frac{r}{\ell}\right) - K_2\left(\frac{r}{\ell}\right)\right]\left(3\sin\theta - \sin 3\theta\right),\end{aligned} \tag{A4}$$

$$\begin{aligned}m_{xz} =& -\frac{\mu b_y w_d}{4\pi\ell^2}\, r\left[K_2\left(\frac{r}{\ell}\right) - K_0\left(\frac{r}{\ell}\right)\right](\sin\theta - \sin 3\theta) \\ & +\frac{2\mu b_y w_d}{\pi r}\left[\frac{2\ell^2}{r^2} - K_2\left(\frac{r}{\ell}\right)\right]\sin 3\theta - \frac{\mu\boldsymbol{\Omega}_z w_d}{\pi}\, K_2\left(\frac{r}{\ell}\right)\sin 2\theta\ ,\end{aligned} \tag{A5}$$

$$
\begin{aligned}
m_{yz} = &-\frac{\mu b_y w_d}{4\pi\ell^2} r\left[K_2\left(\frac{r}{\ell}\right) - K_0\left(\frac{r}{\ell}\right)\right](\cos\theta - \cos 3\theta) - \frac{2\mu b_y w_d}{\pi r}\cos 3\theta \\
&\times\left[\frac{2\ell^2}{r^2} - K_2\left(\frac{r}{\ell}\right)\right] - \frac{2\mu\ell\boldsymbol{\Omega}_z}{\pi}\Big[I_{11}\big(x - w_d/2,\, y\big) - I_{11}\big(x + w_d/2,\, y\big)\Big]\,,
\end{aligned}
\tag{A6}
$$

where

$$
I_{11} = \int_0^\infty \alpha\xi^{-1}\, e^{-\frac{y\,\alpha}{\ell}} \sin\big(\xi x\big)\, d\xi, \quad \alpha \equiv \alpha\big(\xi\big) = \big(1 + \ell^2\xi^2\big)^{1/2}. \tag{A7}
$$

For $y = 0$, the integrals I_{11} in Eq. (A6) are evaluated analytically as

$$
-\frac{2\mu\ell\boldsymbol{\Omega}_z}{\pi}\Big[I_{11}\big(x - w_d/2,\, 0\big) - I_{11}\big(x + w_d/2,\, 0\big)\Big] = \frac{\mu\boldsymbol{\Omega}_z w_d}{\pi}\left[K_0\left(\frac{|x|}{\ell}\right) - K_2\left(\frac{|x|}{\ell}\right)\right]. \tag{A8}
$$

Therefore, the influence functions for the opening mode problem in the displacement-based formulation are obtained in closed form and provided in Eqs. (43)-(45). Further, it is noted that once the two defect densities (Eq. (56)) are evaluated, the stresses and couple-stresses at any point of the cracked body can be obtained using Eqs. (A1)-(A6).

Appendix B

In this Appendix, we provide the closed-form expressions for the singular and hyper-singular integrals involving Chebyshev polynomials that were presented in Section 5. The integrals are calculated in the finite-part sense for $|x| < 1$ (see also Chan et al., 2003). It is mentioned that the integral in Eqs. (B6) and (B12) is derived herein for the first time.

$$
\int_{-1}^{1} \frac{U_n\big(t\big)\big(1 - t^2\big)^{1/2}}{x - t}\, dt = \pi T_{n+1}\big(x\big)\,, \quad n \geq 0\,, \tag{B1}
$$

$$
\text{F.P.}\int_{-1}^{1} \frac{U_n\big(t\big)\big(1 - t^2\big)^{1/2}}{\big(x - t\big)^2}\, dt = -\pi\big(n + 1\big)U_n\big(x\big)\,, \quad n \geq 0\,, \tag{B2}
$$

$$\text{F.P.}\int_{-1}^{1}\frac{U_n\big(t\big)\big(1-t^2\big)^{3/2}}{\big(x-t\big)^2}dt = \\ =\begin{cases}-\dfrac{3\pi}{4}\big[U_0\big(x\big)-U_2\big(x\big)\big], & n=0,\\ -\pi\big[U_1\big(x\big)-U_3\big(x\big)\big], & n=1,\\ \dfrac{\pi}{4}\big[\big(n-1\big)U_{n-2}\big(x\big)-2\big(n+1\big)U_n\big(x\big)+\big(n+3\big)U_{n+2}\big(x\big)\big], & n\geq 2,\end{cases} \tag{B3}$$

$$\text{F.P.}\int_{-1}^{1}\frac{U_n\big(t\big)\big(1-t^2\big)^{3/2}}{\big(x-t\big)^4}dt = \\ =\begin{cases}\pi\ , & n=0,\\ 4\pi U_1\big(x\big)\ , & n=1,\\ 3\pi U_0\big(x\big)+10\pi U_2\big(x\big)\ , & n=2,\\ 4\pi\big[2U_1\big(x\big)+5\pi U_3\big(x\big)\big]\ , & n=3,\\ \dfrac{\pi}{96\big(1-x^2\big)^2}\Big[\big(n^3+6n^2+11n+6\big)U_{n+4}\big(x\big)\\ \qquad -\big(4n^3+18n^2+44n+30\big)U_{n+2}\big(x\big)\\ \qquad +\big(6n^3+18n^2+54n+42\big)U_n\big(x\big) & n\geq 4,\\ \qquad -\big(4n^3+6n^2+20n+18\big)U_{n-2}\big(x\big)\\ \qquad +\big(n^3-n\big)U_{n-4}\big(x\big)\Big]\ ,\end{cases} \tag{B4}$$

$$\int_{-1}^{1}U_n\big(t\big)\big(1-t^2\big)^{1/2}\ln\big(\big|x-t\big|\big)dt\ =\begin{cases}\dfrac{\pi}{4}T_2\big(x\big)-\dfrac{\pi}{2}\ln 2\ , & n=0,\\ -\dfrac{\pi}{2}\left[\dfrac{T_n\big(x\big)}{n}-\dfrac{T_{n+2}\big(x\big)}{n+2}\right], & n\geq 1,\end{cases} \tag{B5}$$

$$\int_{-1}^{1}U_n\big(t\big)\big(1-t^2\big)^{3/2}\ln\big(\big|x-t\big|\big)dt\ =\begin{cases}\dfrac{\pi}{4}\left[T_2\big(x\big)-\dfrac{1}{8}T_4\big(x\big)-\dfrac{3}{2}\ln 2\right], & n=0,\\ -\dfrac{\pi}{4}\left[T_1\big(x\big)-\dfrac{1}{2}T_3\big(x\big)+\dfrac{1}{10}T_5\big(x\big)\right], & n=1,\\ -\dfrac{\pi}{16}\Big[3T_2\big(x\big)-\dfrac{3}{2}T_4\big(x\big)\\ \qquad +\dfrac{1}{3}T_6\big(x\big)-2\ln 2\Big], & n=2,\\ \dfrac{\pi}{8}\Big[\dfrac{T_{n-2}\big(x\big)}{n-2}-\dfrac{3T_n\big(x\big)}{n}\\ \qquad +\dfrac{3T_{n+2}\big(x\big)}{n+2}-\dfrac{T_{n+4}\big(x\big)}{n+4}\Big], & n\geq 3,\end{cases} \tag{B6}$$

where $T_n\big(t\big)$ and $U_n\big(t\big)$ are the Chebyshev polynomials of the first and second kind, respectively.

For $\big|x\big| > 1$, the above integrals are no longer singular and are evaluated according to the following expressions

$$\int_{-1}^{1} \frac{U_n\big(t\big)\big(1-t^2\big)^{1/2}}{x-t}\,dt = \pi\Big[x - \mathrm{sgn}\big(x\big)\big(x^2-1\big)^{1/2}\Big]^{n+1}\ , \qquad n \geq 0\ , \tag{B7}$$

$$\int_{-1}^{1} \frac{U_n\big(t\big)\big(1-t^2\big)^{1/2}}{\big(x-t\big)^2}\,dt = -\pi\big(n+1\big)\left[1 - \frac{\big|x\big|}{\big(x^2-1\big)^{1/2}}\right] \times\Big[x - \mathrm{sgn}\big(x\big)\big(x^2-1\big)^{1/2}\Big]^{n}\ , \qquad n \geq 0\ , \tag{B8}$$

$$\int_{-1}^{1} \frac{U_n\big(t\big)\big(1-t^2\big)^{3/2}}{\big(x-t\big)^2}\,dt = = \begin{cases} -\dfrac{3\pi}{2}\Big[1 - 2x\Big(x - \mathrm{sgn}\big(x\big)\big(x^2-1\big)^{1/2}\Big)\Big], & n = 0, \\ \pi\Big[x - \mathrm{sgn}\big(x\big)\big(x^2-1\big)^{1/2}\Big]^{n+1}\Big[2x - \big(n+1\big)\mathrm{sgn}\big(x\big)\big(x^2-1\big)^{1/2}\Big], & n \geq 1, \end{cases} \tag{B9}$$

$$\int_{-1}^{1} \frac{U_n\big(t\big)\big(1-t^2\big)^{3/2}}{\big(x-t\big)^4}\,dt = \frac{\pi\big(n+1\big)\mathrm{sgn}\big(x\big)\Big[x - \mathrm{sgn}\big(x\big)\big(x^2-1\big)^{1/2}\Big]^{n+1}}{6\big(x^2-1\big)^{3/2}} \times\Big[3 - \big(n^2+2n+3\big)\big(x^2-1\big) + 3\big(n+1\big)x\,\mathrm{sgn}\big(x\big)\big(x^2-1\big)^{1/2}\Big], \qquad n \geq 0\ , \tag{B10}$$

$$\int_{-1}^{1} U_n\big(t\big)\Big(1-t^2\Big)^{1/2}\ln\big(\big|x-t\big|\big)dt \;=\; \begin{cases} \dfrac{\pi}{2}\Big[x^2-\big|x\big|\big(x^2-1\big)^{1/2} & \\ \quad +\ln\Big(\big|x\big|+\big(x^2-1\big)^{1/2}\Big)-\ln 2-\dfrac{1}{2}\Big], & n=0, \\ -\dfrac{\pi}{2}x^{-n}\left[1+\dfrac{\big(x^2-1\big)^{1/2}}{\big|x\big|}\right]^{-n} & \\ \quad \times\left[\dfrac{1}{n}-\dfrac{1}{\big(n+2\big)x^2}\left(1+\dfrac{\big(x^2-1\big)^{1/2}}{\big|x\big|}\right)^{-2}\right], & n\geq 1, \end{cases} \tag{B11}$$

$$\int_{-1}^{1} U_n\big(t\big)\Big(1-t^2\Big)^{3/2}\ln\big(\big|x-t\big|\big)dt \;=$$

$$\begin{cases} -\dfrac{\pi}{8}\Big[2x^4-6x^2-x\big(2x^2-5\big)\mathrm{sgn}\big(x\big)\big(x^2-1\big)^{1/2} & \\ \quad -3\ln\Big(x+\mathrm{sgn}\big(x\big)\big(x^2-1\big)^{1/2}\Big)\Big]-\dfrac{3\pi}{8}\Big(\ln 2+\dfrac{3}{4}\Big), & n=0, \\ -\dfrac{\pi}{4}\left[\dfrac{8}{5}x^5-4x^3+3x-\dfrac{8}{5}\mathrm{sgn}\big(x\big)\big(x^2-1\big)^{5/2}\right], & n=1, \\ -\dfrac{\pi}{24}\big[16x^6-42x^4+36x^2 & \\ \qquad +x\big(16x^4+34x^2-21\big)\mathrm{sgn}\big(x\big)\big(x^2-1\big)^{1/2} & n=2, \\ \qquad +3\ln\Big(x+\mathrm{sgn}\big(x\big)\big(x^2-1\big)^{1/2}\Big)\Big]+\dfrac{\pi}{8}\Big(\ln 2+\dfrac{29}{12}\Big), & \\ \dfrac{\pi}{\big(n^3-4n\big)\big(n+4\big)}\Big[x-\mathrm{sgn}\big(x\big)\big(x^2-1\big)^{1/2}\Big]^n & \\ \qquad \times\big[-nx^2\big(n^2x^2-4x^2-2n^2-3n+8\big) & n\geq 3. \\ \qquad +nx\big(n^2x^2-4x^2-n^2+10\big)\mathrm{sgn}\big(x\big)\big(x^2-1\big)^{1/2} & \\ \qquad -\big(n^3+3n^2-4n-6\big)\big], & \end{cases} \tag{B12}$$

References

Atkinson, C., Leppington, F.G., 1974. Some calculations of the energy-release rate G for cracks in micropolar and couple-stress elastic media. Int. J. Fract. 10, 599-602.

Atkinson, C., Leppington, F.G., 1977. The effect of couple stresses on the tip of a crack. Int. J. Solids Struct. 13, 1103-1122.

Ballarini, R., Denda, M., 1988. The interaction between a crack and a dislocation dipole. Int. J. Fract. 37, 61-71.

Baxevanakis, K.P., Gourgiotis, P.A., Georgiadis, H.G., 2017a. Interaction of cracks with dislocations in couple-stress elasticity. Part I: Opening mode. Int. J. Solids Struct. 118-119, 179-191.

Baxevanakis, K.P., Gourgiotis, P.A., Georgiadis, H.G., 2017b. Interaction of cracks with dislocations in couple-stress elasticity. Part II: Shear modes. Int. J. Solids Struct. 118-119, 192-203.

Bjerkén, C., Melin, S., 2003. A tool to model short crack fatigue growth using a discrete dislocation formulation. Int. J. Fatigue 25, 559-566.

Burridge, R., 1976. An influence function for the intensity factor in tensile fracture. Int. J. Eng. Sci. 14, 725-734.

Chan, Y.-S., Fannjiang, A.C., Paulino, G.H., 2003. Integral equations with hypersingular kernels – theory and applications to fracture mechanics. Int. J. Eng. Sci. 41, 683-720.

Chan, Y.-S., Paulino, G.H., Fannjiang, A.C., 2001. The crack problem for nonhomogeneous materials under antiplane shear loading – a displacement based formulation. Int. J. Solids Struct. 38, 2989-3005.

Dai, D.N., 2002. Modelling cracks in finite bodies by distributed dislocation dipoles. Fatigue Fract. Eng. Mater. Struct. 25, 27-39.

Eshelby, J.D., 1951. The force on an elastic singularity. Phil. Trans. R. Soc. Lond. A 244, 87-112.

Fisher, B., 1971. The product of distributions. Q. J. Math. 22, 291-298.

Freund, L.B., 1972. Energy flux into the tip of an extending crack in an elastic solid. J. Elasticity 2, 341-349.

Gel′fand, I., Shilov, G., 1964. Generalized Functions, Vol. 1. Academic Press, New York.

Georgiadis, H.G., 2003. The Mode III crack problem in microstructured solids governed by dipolar gradient elasticity: Static and dynamic analysis. J. Appl. Mech. 70, 517-530.

Gilman, J., 1964. Influence of dislocation dipoles on physical properties. Disc. Faraday Soc. 38, 123-137.

Gourgiotis, P., Piccolroaz, A., 2014. Steady-state propagation of a mode II crack in couple stress elasticity. arXiv: 1304.7444.

Hills, D.A., Kelly, P.A., Dai, D.N., Korsunsky, A.M., 1996. Solution of crack problems: the distributed dislocation technique. Kluwer Academic Publishers.

Huang, M., Rivera Díaz del Castillo, P.E.J., Li, Z., 2006. Edge dislocation dipole emission from a blunt crack tip and its morphological effects. Scr. Mater. 54, 649-653.

Huang, Y., Zhang, L., Guo, T.F., Hwang, K.C., 1997. Mixed mode near-tip fields for cracks in materials with strain-gradient effects. J. Mech. Phys. Solids 45, 439-465.

Kobayashi, S., Ohr, S.M., 1980. In situ fracture experiments in b.c.c. metals. Philos. Mag. A 42, 763-772.

Koiter, W., 1964. Couple stresses in the theory of elasticity. Parts I and II, Nederl. Akad. Wetensch. Proc. Ser. B, pp. 17-29.

Korsunsky, A., Hills, D., 1995. The solution of plane crack problems by dislocation dipole procedures. J. Strain Anal. Eng. Des. 30, 21-27.

Korsunsky, A., Hills, D., 1996. The solution of crack problems by using distributed strain nuclei. P. I. Mech. Eng. C-J. Mec. 210, 23-31.

Kroupa, F., 1965. Dislocation dipoles of infinitesimal width. Czech J Phys 15, 896-900.

Kroupa, F., 1966. Dislocation dipoles and dislocation loops. J. Phys. Colloq. 27, C3-154-C153-167.

Lin, K.M., Hu, C.T., Lee, S., 1993. Screw dislocation dipoles near an internal crack. Eng. Fract. Mech. 45, 321-331.

Lubarda, V.A., 2003. The effects of couple stresses on dislocation strain energy. Int. J. Solids Struct. 40, 3807-3826.

Majumdar, B.S., Burns, S.J., 1981. Crack tip shielding – an elastic theory of dislocations and dislocation arrays near a sharp crack. Acta Metall. 29, 579-588.

Mindlin, R.D., 1963. Influence of couple-stresses on stress concentrations. Exp. Mech. 3, 1-7.

Mindlin, R.D., Tiersten, H.F., 1962. Effects of couple-stresses in linear elasticity. Arch. Ration. Mech. Anal. 11, 415-448.

Monegato, G., 1994. Numerical evaluation of hypersingular integrals. J. Comput. Appl. Math. 50, 9-31.

Rice, J.R., Thomson, R., 1974. Ductile versus brittle behaviour of crystals. Philos. Mag. 29, 73-97.

Sternberg, E., Muki, R., 1967. The effect of couple-stresses on the stress concentration around a crack. Int. J. Solids Struct. 3, 69-95.

TerMaath, S.C., Phoenix, S.L., Hui, C.Y., 2006. A technique for studying interacting cracks of complex geometry in 2D. Eng. Fract. Mech. 73, 1086-1114.

Tetelman, A.S., 1962. Dislocation dipole formation in deformed crystals. Acta Metall. 10, 813-820.

Thomson, R.M., 1987. Physics of fracture. J. Phys. Chem. Solids 48, 965-983.

Toupin, R.A., 1962. Elastic materials with couple-stresses. Arch. Ration. Mech. Anal. 11, 385-414.

Wang, S.-D., Lee, S., 1992. Mechanical equilibrium of an edge dislocation dipole near a crack tip. Int. J. Fract. 57, 317-324.

Wang, S.-D., Lee, S., 1993. Edge dislocation dipoles near a semi-infinite crack tip. Eng. Fract. Mech. 46, 297-309.

Weertman, J., 1996. Dislocation based Fracture Mechanics. World Scientific, Singapore.

Yavuz, A.K., Phoenix, S.L., TerMaath, S.C., 2006. An accurate and fast analysis for strongly interacting multiple crack configurations including kinked (V) and branched (Y) cracks. Int. J. Solids Struct. 43, 6727-6750.

Zhang, L., Huang, Y., Chen, J.Y., Hwang, K.C., 1998. The mode III full-field solution in elastic materials with strain gradient effects. Int. J. Fract. 92, 325-348.